ELSEVIER

Contents lists available at ScienceDirect

Acta Materialia

journal homepage: www.elsevier.com/locate/actamat



Full length article

Dislocation \leftrightarrow twin transmutations during interaction between prismatic slip and $\{10\overline{1}1\}$ twin in magnesium



Peng Chen^{a,b,*}, Jamie Ombogo^{a,b}, Bin Li^{a,b,*}

- ^a Department of Chemical and Materials Engineering, University of Nevada, Reno, USA
- ^b Nevada Institute for Sustainability, University of Nevada, Reno, USA

ARTICLE INFO

Article History: Received 14 September 2019 Revised 5 January 2020 Accepted 5 January 2020 Available online 8 January 2020

Keywords: Magnesium Contraction twinning Prismatic dislocation Twin-slip interaction

ABSTRACT

Very unusual and interesting interaction between matrix prismatic dislocations and $\{10\overline{1}1\}$ twin boundaries (TBs) in Magnesium (Mg) was observed in atomistic simulations. When the first prismatic dislocation impinged on the TB, the incoming dislocation was transmuted into a thin layer of $\{11\overline{2}1\}$ twin inside the $\{10\overline{1}1\}$ twin. When successive prismatic dislocations on the same slip plane impinged on the same location at the $\{10\overline{1}1\}$ TB, the $\{11\overline{2}1\}$ twin kept growing toward the opposite $\{10\overline{1}1\}$ TB. Eventually, the $\{11\overline{2}1\}$ twin reached the opposite TB and was then transmuted back to prismatic dislocations that exited the $\{10\overline{1}1\}$ twin and glided into the matrix. Hence, the matrix prismatic dislocations temporarily lose their dislocation identity during twin-slip interaction and then resume their dislocation identity after the interaction is complete. The net effect of these interactions is that the matrix prismatic dislocations transmit across the $\{10\overline{1}1\}$ twin. Lattice correspondence analysis for $\{10\overline{1}1\}$ twinning was performed to understand the mechanism of the interactions. The results show that, the prismatic slip plane is exactly the corresponding plane of $\{11\overline{2}1\}$ twinning. Such a correspondence is consistent with the crystallographic calculations based on classical twinning theory.

© 2020 Acta Materialia Inc. Published by Elsevier Ltd. All rights reserved.

1. Introduction

When a matrix dislocation impinges on a twin boundary (TB), interaction occurs. In general, such interaction processes are dependent on characteristics of the twinning mode, dislocation type and grain size, as well as loading condition [1–4]. In cubic metals, when a TB interacts with matrix dislocations, several scenarios may occur: (1) TBs act as a barrier to dislocation slip [2,5], resulting in strain hardening; (2) TBs serve as a dislocation sink, i.e., dislocations are absorbed by the TBs [6,7]; (3) matrix dislocations can transmit through the TB into the twin and glide on the corresponding slip plane [3,8,9]; (4) a matrix dislocation can dissociate into a twinning dislocation and leaves a residual dislocation at the TB [2,8,10].

Twinning and dislocation slip are the major deformation modes in plastic deformation of hexagonal close-packed (HCP) metals. Due to the low symmetry in crystal structures, deformation twinning accommodates the plastic strain along the c-axis which cannot be achieved by basal and prismatic dislocations. In magnesium (Mg), the $\{10\overline{1}2\}$ extension twinning and $\{10\overline{1}1\}$ contraction twinning are the two major modes, and have been studied experimentally and computationally [11-14]. In terms of twin-slip interaction, the interaction mechanisms between $\{10\overline{1}2\}$ extension TBs and matrix dislocations

E-mail addresses: pengchen@tamu.edu (P. Chen), binl@unr.edu (B. Li).

have been investigated by a number of researchers [15-22]. To account for the sharp increase in hardening rate during plastic deformation of single crystal and highly textured polycrystal Mg, interaction between matrix dislocations and $\{10\overline{1}2\}$ TBs was assumed as a key contributor [15]. However, Capolungo et al. [16] showed that the stored dislocations in matrix by pre-strainning do not increase the resistance of the propagation of $\{10\overline{1}2\}$ TBs. Chen et al. [17] showed similar behavior in an extruded AZ31 Mg alloy. Recently, Chen et al. [18] systematically investigated how matrix dislocations interact with $\{10\overline{1}2\}$ TBs. They showed that matrix basal and prismatic dislocations can be transmuted to prismatic and basal dislocations in the twin, only when their Burgers vectors are parallel to the zone axis of the twins. In contrast, when the Burgers vector of the matrix dislocations is non-parallel to the zone axis, the $\{10\overline{1}2\}$ TBs act as a dislocation sink that absorbs the dislocations, irrespective of basal, prismatic or pyramidal dislocations. These simulation results well explain why $\{10\overline{1}2\}$ twin-slip interaction only contributes negligibly to work hardening in Mg and Mg alloys [17].

Unlike $\{10\overline{1}2\}$ extension twinning which exhibits many nonclassical characteristics [23-27], $\{10\overline{1}1\}$ contraction twinning is normally activated at high stress/strain levels near fracture and it has been considered a key player in fracture of Mg alloys. This twinning mode is mediated by zonal twinning dislocations [28] and can be well described by classical twinning theory [29]. When a tensile load is applied along the extrusion direction of a Mg alloy with a strong basal texture, the dominant deformation mechanism is prismatic slip

^{*} Corresponding authors at: Department of Chemical and Materials Engineering, University of Nevada, Reno, USA.

followed by contraction twinning and pyramidal slip [30]. In this case, interaction between contraction twins and prismatic slip can be expected. Kalidindi et al. [31] reported that the interaction between $\{10\overline{1}1\}$ twins and dislocations effectively contributes to strain hardening in a Mg alloy by decreasing the mean free path of dislocations, but no interaction mechanisms were provided. Recently, Peng et al. [32,33] developed a novel Mg alloy with hierarchical contraction twin structure which presents strong blocking effect to dislocation motion and improves the yield strength. Yuasa et al. [34] reported that a screw basal dislocation can be absorbed into a $\{10\overline{1}1\}$ TB and split into two twinning dislocations. Li et al. [35] also studied how basal dislocations interact with a $\{10\overline{1}1\}$ TB and showed that pyramidal stacking faults are generated inside the twin when a basal dislocation impinges on the $\{10\overline{1}1\}$ TB. However, interaction of $\{10\overline{1}1\}$ TB with other matrix dislocations, e.g., prismatic dislocations, have not been reported.

The aim of this work is to study how matrix prismatic dislocations interact with $\{10\overline{1}1\}$ TBs in pure Mg by using atomistic simulations. Very interesting and unusual transmutations were observed. Lattice correspondence analysis was performed to understand the mechanism of such twin-slip interaction. The results obtained provide new insight on the deformation behavior of Mg and other hcp metals.

2. Simulation method

The embedded atom method (EAM) potential [36,37] for Mg-Al binary system was used in this work. This EAM potential was well developed by Liu et al. [38], and have been used in numerous atomistic simulations of deformation behavior of Mg and Mg-Al alloys [13,18,39–41].

The initial configuration for simulating interaction between prismatic dislocations and a $\{10\overline{1}1\}$ contraction twin boundary (TB) in magnesium is shown in Fig. 1a. The 3D simulation box of single crystal Mg has a dimension of $25.5 \times 16.5 \times 15.5 \text{ nm}^3$, containing a total of 288,000 atoms. The simulation system was fully relaxed before the external tensile strain was applied. The tensile load was applied along the $[2\overline{11}0]$ direction, which was generated by moving the atoms on the right free surface away from the box at a constant displacement rate of $a_0/10$, 000 per timestep, where $a_0=0.32$ nm is the lattice constant of Mg. The timestep size equals 3 fs. The corresponding strain rate is 4.2×10^9 /s. The temperature was maintained at 100 K during simulation. Free surfaces were applied to all three dimensions. Note that no pre-existing dislocations and twins were constructed in our simulation. Dislocations and deformation twins will be generated by deformation. This ensures that no artifacts would be generated. The

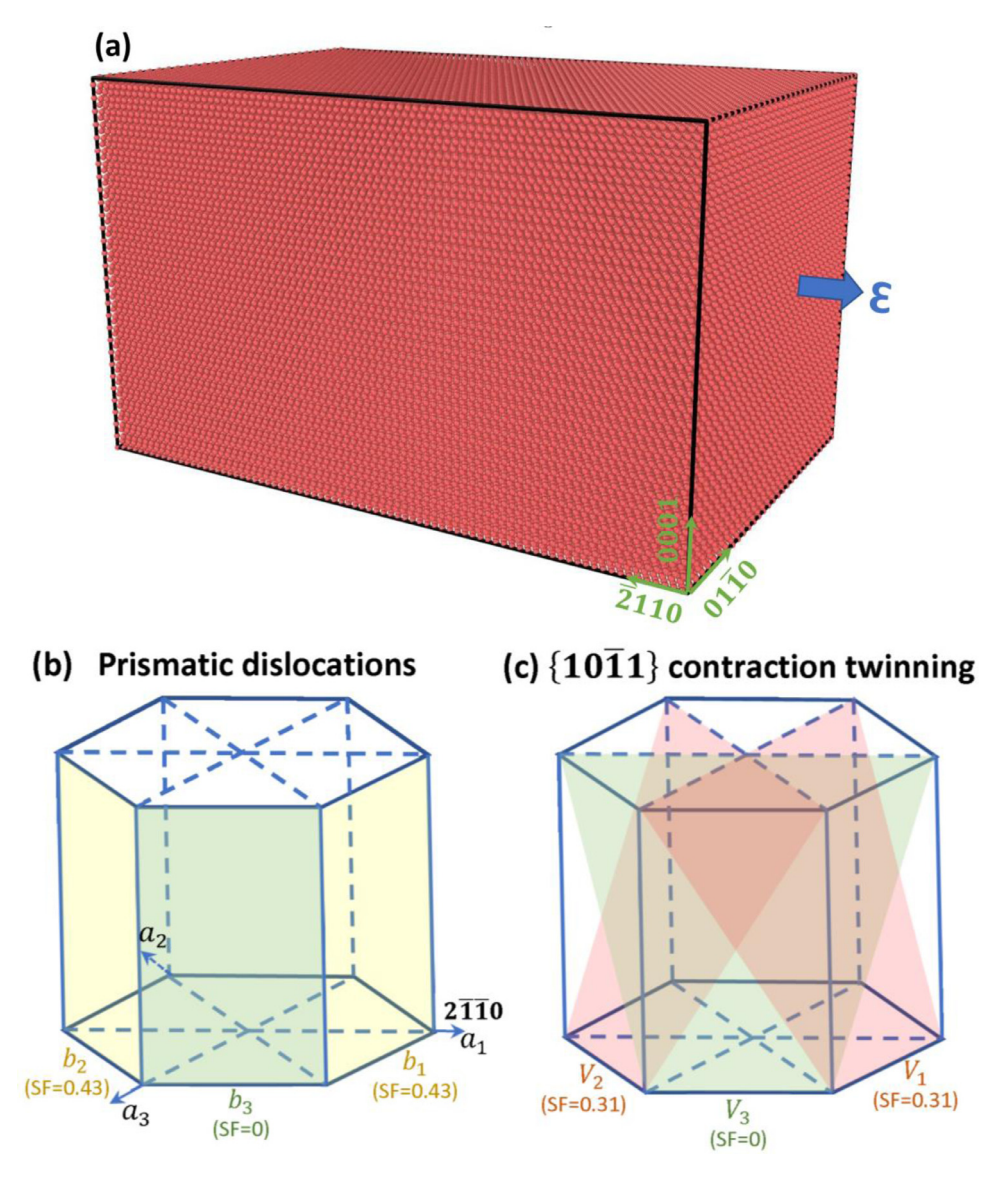


Fig. 1. (a) Initial, perfect single crystal Mg for simulating interaction between prismatic slip and $\{10\overline{1}1\}$ twin. A tensile load was applied along the $[2\overline{1}\overline{1}0]$. This loading condition disfavors $\{10\overline{1}2\}$ twinning and basal slip, but favors prismatic slip and $\{10\overline{1}1\}$ twinning. (b) The prismatic slip systems and their Schmid factors (SF). (c) The $\{10\overline{1}1\}$ twinning systems and their Schmid factors.

visualization tool Ovito [42] was used to analyze the simulation results. Common neighbor analysis (CNA) [43] was used to distinguish the crystal structures and lattice defects.

The coordinate system of the hcp unit cell is shown in Fig. 1b and 1c, which displays the prismatic slip systems and $\{10\overline{1}1\}$ twinning planes, along with the Schmid factors (SFs) under the applied loading condition. The basal slip has zero Schmid factor, so no basal dislocations will be activated. For the prismatic slip systems, a dislocation with Burgers vector $b_1^- = \frac{1}{3}[2\overline{110}]$ also has zero Schmid factor. But for prismatic dislocations with Burgers vector $b_2^- = \frac{1}{3}[\overline{1120}]$ and $b_3^- = \frac{1}{3}[\overline{1120}]$, the Schmid factor equals ~0.43. Thus, these prismatic dislocations can be activated. For the twin variant with zone axis V_3 and its co-zone variant, the Schmid factor equals zero. Twin variants with zone axes V_1 and V_2 and their co-zone variants have a large Schmid factor ~0.31. This coordinate system will be used for lattice correspondence analysis which is critically important in understanding the mechanism for interaction between prismatic dislocations and $\{10\overline{1}1\}$ twins.

3. Results

Because of the low symmetry of hexagonal-close-packed (hcp) structures, activation of deformation modes during plastic deformation of Mg alloys are dependent on the loading direction with respect to the crystal orientation [44]. In the present simulation, the tensile strain was along the $[2\overline{11}0]$ direction, so the Schmid factor of the basal dislocations equals zero, and no basal slip should be activated.

The loading condition also disfavors $\{10\overline{1}2\}$ extension twinning but favors prismatic slip and $\{10\overline{1}1\}$ contraction twinning.

Fig. 2 shows 3D views of a $(10\overline{1}1)$ twin and a prismatic dislocation. As shown in Fig. 2a, when the tensile strain was increased to a critical value, a contraction twin was nucleated and grew. In this plot, the whole box is tilted by ~60° around the c-axis of the parent, such that the zone axis of the twin, i.e. $[\overline{1}2\overline{1}0]$, is nearly perpendicular to the figure plane. It can be seen that this variant is indeed a $(10\overline{1}1)$ twin. It can also be observed that the TB is mostly coherent with steps on it. This is consistent with previous simulation results [28] and high resolution TEM observations [29]. Li and Ma [28] showed that the onelayer steps on the TB are immobile, and the two-layer steps are zonal twinning dislocations that are stable and mobile, whereas the fourlayer steps are mobile but tend to dissociate into two two-layer steps. Additionally, two types of basal stacking faults can be observed inside the $(10\overline{1}1)$ twin. It is worth noting that these stacking faults are fundamentally different: the single-layered fault (in green) is generated by large atomic shuffles and have nothing to do with Shockley partial dislocations [45], and they are defined "partial stacking faults" [26,27] because only those atoms on every other basal plane are displaced. In sharp contrast, the double-layered stacking fault is created by a Shockley partial dislocation [18]. As the deformation proceeds, the $(10\overline{1}1)$ twin continues growing. Fig. 2b shows a 3D view of the system when those atoms of perfect HCP structure are removed. It is observed that the two $(10\overline{1}1)$ twin boundaries (TBs) are coherent. A prismatic dislocation gliding in the matrix toward the TB is also revealed.

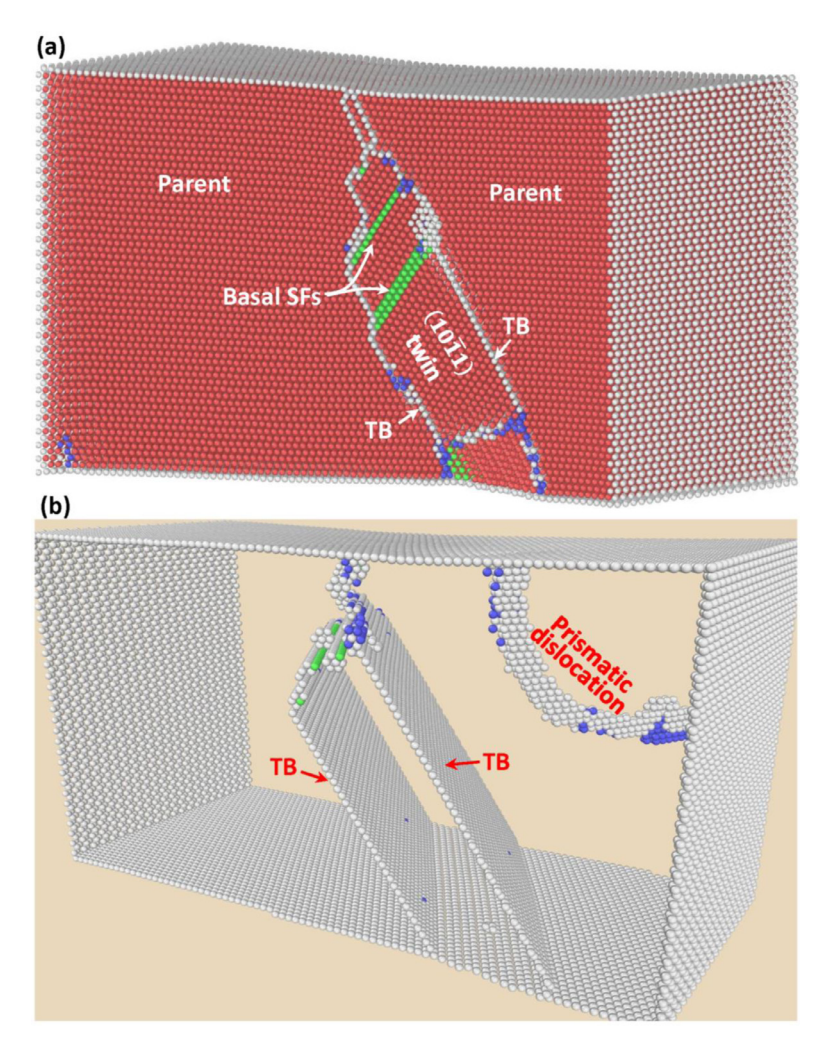


Fig. 2. (a) As the tensile strain was increased to a critical value, a (1011) twin was nucleated and grew. (b) 3D view of the (1011) twin boundaries (TBs) which are coherent. Atoms in the perfect hcp lattice are hidden. A prismatic dislocation gliding in the matrix toward the TB is also revealed.

In Fig. 3a, as the tensile strain increases, the prismatic dislocation is gliding toward the TB. To determine its Burgers vector of this prismatic dislocation, the crystal box is tilted such that the slip plane is edge-on. Then a Burgers circuit is drawn around the dislocation (the white and blue atoms, Fig. 3b). It is seen that the dislocation is on the $(1\overline{1}\,00)$ prismatic plane, and its Burgers vector is determined as $\frac{1}{3}[\overline{11}\,20]$. Fig. 3c schematically shows the $(1\overline{1}\,00)$ prismatic slip and the $(10\overline{1}\,1)$ twin. It can be seen that the prismatic slip plane and the twinning plane intersect. Thus, interaction between the prismatic dislocation and the TB will occur. Notably, the Burgers vector of this prismatic dislocation is non-parallel to the zone axis of the $(10\overline{1}\,1)$ twin.

The process of twin-slip interaction is shown in Fig. 4. The first prismatic dislocation glides, approaches and eventually impinges on the TB (Fig. 4a). This dislocation is designated as the "1st prismatic dislocation" because later on a second prismatic dislocations (see below) nucleates, glides and then impinges on the TB at the same location. To record the energy evolution during twin-slip interaction between the prismatic dislocations and (1011) TBs, a boxed region located at the right TB was selected (Fig. 4a), and the average potential energy of the selected atoms were computed vs. simulation time. As the 1st prismatic dislocation touches the TB, a new structure (indicated by the dashed red circle) is created inside the twin (Fig. 4b). This new structure not only grows toward the interior of the (1011) twin (Fig. 4c), but also extends along the trace of the impingement (Fig. 4d). As analyzed below, this new structure inside the twin is actually a

 $(2\overline{11}1)[\overline{2}116]$ twin whose parent is the $(10\overline{1}1)$ twin. Eventually, the 1st prismatic dislocation completes the interaction, disappears from the matrix but creates a $(2\overline{11}1)$ twin inside the $(10\overline{1}1)$ twin. Similarly, another region, i.e. box 2 (Fig. 4d) which contains a part of the $(2\overline{11}1)$ twin was selected to compute the energy evolution.

To analyze the new structure that is created by the twin-slip interaction, the $(10\overline{1}\,1)$ twin is tilted such that this structure is viewed nearly along the trace of the dislocation line impinging on the TB (Fig. 5a). The twin-slip interaction creates a step on the TB. It can be seen that this new structure is only several atomic layers in thickness and height. Another tilting is then performed such that the viewing direction is along the $[01\overline{1}0]$, i.e. the zone axis for $(2\overline{1}\overline{1}1)$ twins (Fig. 5b). In this viewing direction, the interface between the new structure (in white) and the $(10\overline{1}1)$ twin (in red) is edge-on. Thus, the new structure that is created by the twin-slip interaction is indeed a $(2\overline{1}\overline{1}1)$ twin whose parent is the $(10\overline{1}1)$ twin. But the thickness of the $(2\overline{1}\overline{1}1)$ twin only contains three atomic layers. Hence, the prismatic dislocation in the parent is transmuted to a $(2\overline{1}\overline{1}1)$ twin inside the $(10\overline{1}1)$ twin.

As the deformation continues, the $(10\overline{1}\,1)$ twin grows and more prismatic dislocations are generated and glide toward the TB. Fig. 6a shows a second prismatic dislocation nucleates and glides on the same slip plane of the first one and interacts with the TB at the same location. As the top portion of the 2nd prismatic dislocation impinges on and interacts with the TB, this interaction causes the $(2\overline{11}\,1)$ twin to further grow inside the $(10\overline{1}\,1)$ twin toward the opposite TB

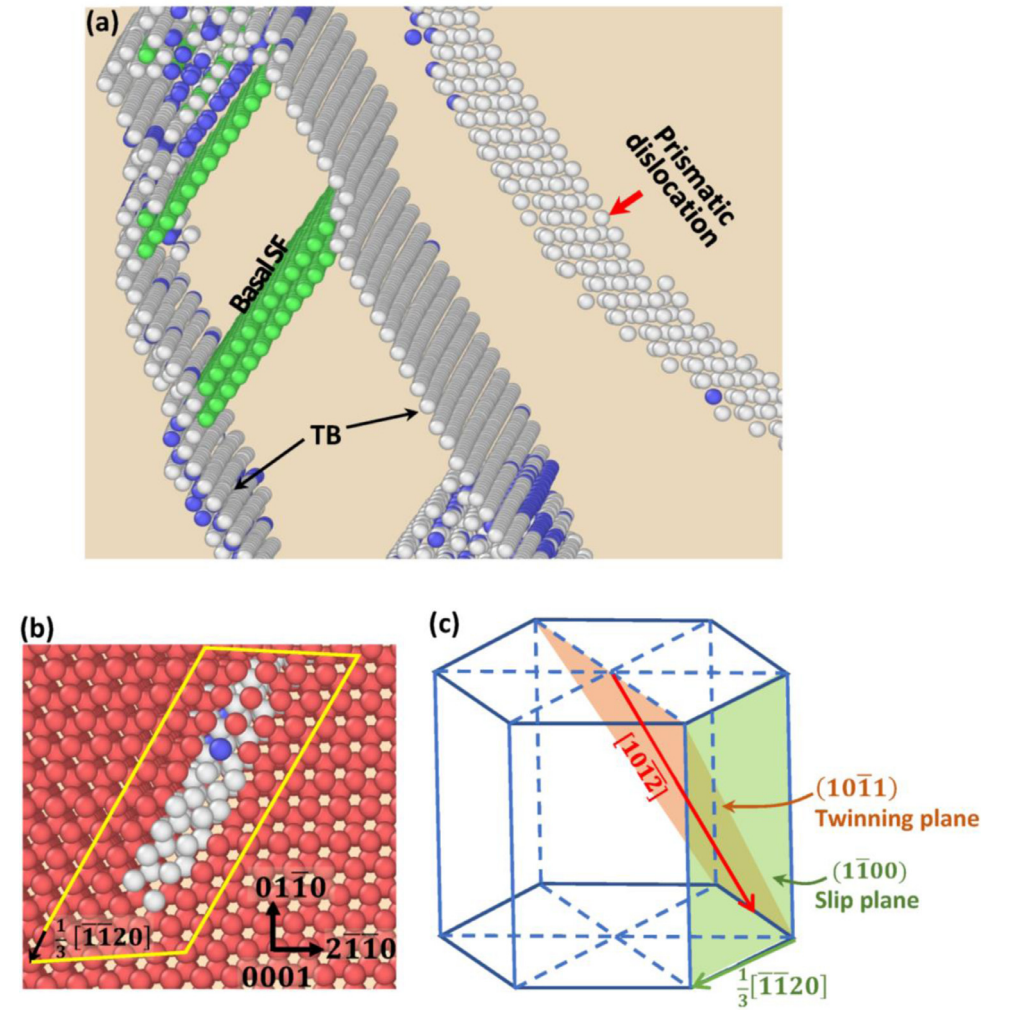


Fig. 3. (a) The prismatic dislocation is approaching the TB. (b) Burgers circuit analysis shows that the $(1\overline{1}00)$ prismatic dislocation has a Burgers vector of $\frac{1}{3}[\overline{1}\overline{1}20]$. (c) Crystallography of the $(1\overline{1}00)$ slip system and the $(10\overline{1}1)$ twinning system.

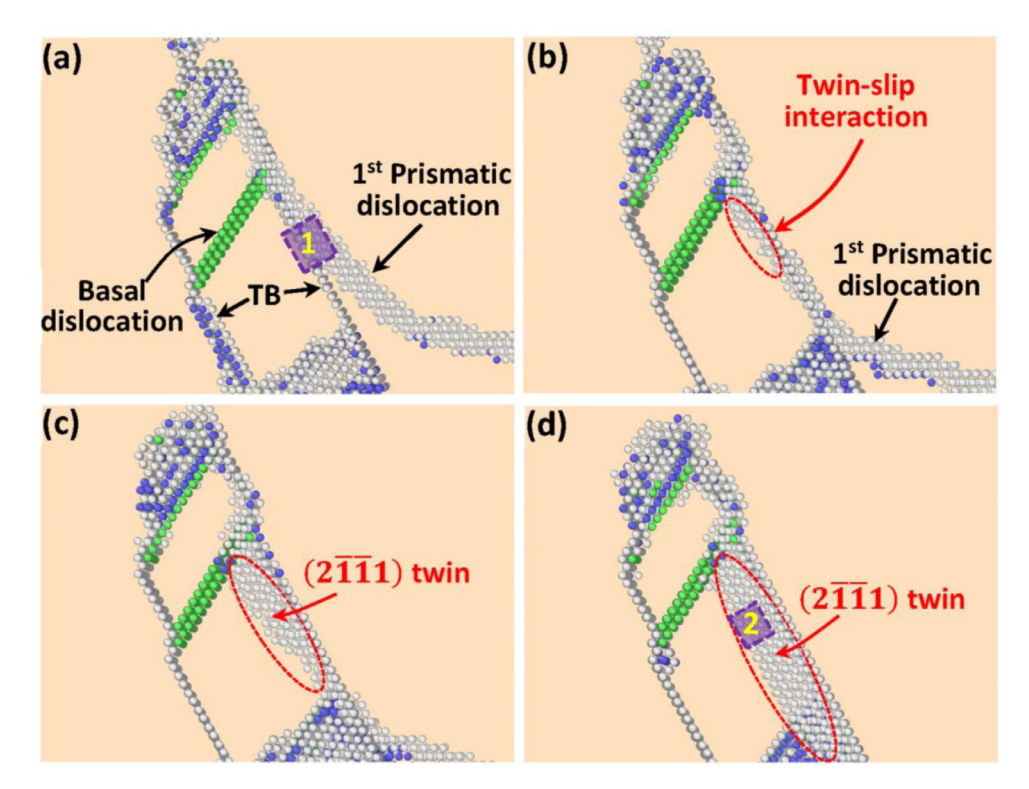


Fig. 4. Interaction between the prismatic dislocation and the $(10\overline{1}1)$ twin boundary (TB) in time sequence. The TBs are edge-on. (a) The prismatic dislocation impinges on the TB. A boxed region was selected at the TB to compute the energy evolution during twin-slip interaction. (b) The prismatic dislocation interacts with the twin and creates a structure (indicated by the dashed red circle) inside the twin. As analyzed in Fig. 5, this structure is actually a $(2\overline{1}\overline{1}1)$ twin whose parent is the $(10\overline{1}1)$ twin. (c) The $(2\overline{1}\overline{1}1)$ twin grows into the $(10\overline{1}1)$ twin. (d) The $(2\overline{1}\overline{1}1)$ twin lengthens along the TB. Another boxed region containing part of the $(2\overline{1}\overline{1}1)$ twin was selected to compute the energy evolution.

(Fig. 6b). Eventually, the $(2\overline{11}1)$ twin grows and reaches the opposite $(10\overline{1}1)$ TB (Fig. 6c). In Fig. 6c, a region located at the opposite TB (box 3) was selected to compute the energy evolution during the interaction between the $(2\overline{11}1)$ twin and TB. When the 2nd prismatic dislocation completes its interaction with the $(10\overline{1}1)$ twin, the $(2\overline{11}1)$ twin detaches from the right $(10\overline{1}1)$ TB on which the prismatic dislocations first impinge (Fig. 6d). What happens next is very interesting. A prismatic dislocation, which has the same Burgers vector as the incoming prismatic dislocations, is formed on the opposite $(10\overline{1}1)$ TB and glides away from the TB toward the free surface (Fig. 6e). As this dislocation is exiting the TB, the $(2\overline{11}1)$ twin gradually shrinks and eventually disappears inside the $(10\overline{1}1)$ twin (Fig. 6f).

To better reveal the twin \rightarrow dislocation transmutation during twin-slip interaction as shown in Fig. 6, the $(10\overline{1}1)$ twin is tilted while the TBs are maintained edge-on, and the slip plane of the prismatic dislocations in the matrix is also edge-on. Fig. 7 shows the edge-on views of the interaction between the 2nd prismatic dislocation and the $(10\overline{1}1)$ TBs in time sequence. In Fig. 7a, the 2nd prismatic dislocation impinges on the $(10\overline{1}1)$ TB at the same location as does the 1st prismatic dislocation. It can be clearly seen that, the impingement of the 2nd prismatic dislocation on the TB causes the $(2\overline{1}\overline{1}1)$ twin to thicken and grow toward the opposite $(10\overline{1}1)$ TB (Fig. 7b and 7c). As the interaction continues, the $(2\overline{11}1)$ twin further grows and reaches the opposite $(10\overline{1}1)$ TB. At this time, an exiting dislocation is formed at the TB (Fig. 7d), and this dislocation is gliding away from the TB toward the free surface of the system (Fig. 7e). As the first exiting dislocation reaches and disappears at the free surface, a 2nd exiting dislocation is formed and glide toward the free surface as well. The $(2\overline{1}\overline{1}1)$ twin gradually disappears from the inside of the $(10\overline{1}1)$ twin as the 2nd exiting dislocation is gliding away (Fig. 7f). Eventually, the twin-slip interaction is completed, and the $(2\overline{1}\overline{1}1)$ twin and matrix prismatic dislocations all disappear.

In Fig. 8a, the lattice is tilted such that the $(2\overline{11}1)$ TBs are edge-on. It can be seen that the $(2\overline{11}1)$ twin slightly grows (compared to

Fig. 5b) as the 2nd prismatic dislocation is interacting with TB. Fig. 8b shows the slip plane of the exiting prismatic dislocation. Obviously, this dislocation is on the prismatic plane of the parent and has the same Burgers vector of the incoming prismatic dislocations in Figs. 4, 6 and 7. Hence, the whole interaction process can be expressed as: $(1\overline{1}00)_{dislocation} \rightarrow (2\overline{1}\overline{1}1)_{puin} \rightarrow (1\overline{1}00)_{dislocation}$.

 $(1\overline{1}00)_{dislocation} \rightarrow (2\overline{11}1)_{twin} \rightarrow (1\overline{1}00)_{dislocation}.$ Fig. 5a shows that a step is created when the first dislocation interacts with the $(10\overline{1}1)$ TB. When a matrix dislocation interacts with a twin boundary, a residual dislocation and a step could be left on the TB [2,8,10]. To reveal how the step in Fig. 5a evolves during twin-slip interaction, another set of close-up views is provided in Fig. 9. Before the prismatic dislocation impinges on the TB (Fig. 9a), the TB is coherent. After the prismatic dislocation impinges and interacts with the TB, a one-layer step is left at the TB (Fig. 9b). The onelayer step can clearly be seen after the dislocation is transmuted into the $(2\overline{11}1)$ twin (Fig. 9c). At this time, a double layered zonal dislocation glides toward the step from the lower right side. However, this zonal dislocation is a detwinning dislocation and it shrinks the twin by two $(10\overline{1}1)$ planes. The Burgers vector of this detwinning dislocation equals $-b_T = \frac{4\gamma^2 - 9}{2(4\gamma^2 + 3)} \left[\overline{1}012 \right]$ (γ is the c/a ratio 1.624 for Mg) [46]. This causes the step to switch side due to the local detwinning (Fig. 9d). As the 2nd prismatic dislocation interacts with the TB (Fig. 9e), the one-layer step is eliminated by this 2nd dislocation and the TB resumes coherency (Fig. 9f). The overall reaction of the two prismatic dislocations and the detwinning dislocation can be described as: $2 \times \frac{1}{3} \left[\overline{11}20\right] + \frac{4\gamma^2 - 9}{2(4\gamma^2 + 3)} \left[\overline{10}12\right]$, which eliminates the steps on the TB.

Fig. 10 shows the evolution of the step on the opposite side of the $(10\overline{1}1)$ TB when the $(2\overline{1}\overline{1}1)$ twin interacts with the TB and transmutes back into prismatic dislocation in the parent. The TB is initially coherent before the $(2\overline{1}\overline{1}1)$ twin impinges on it (Fig. 10a). As the $(2\overline{1}1)$ twin reaches the TB and is transmuted to prismatic dislocation, a one-layer step is created on the TB (Fig. 10b). The one-layer step retains after the 1st dislocation completely exits the $(10\overline{1}1)$ twin

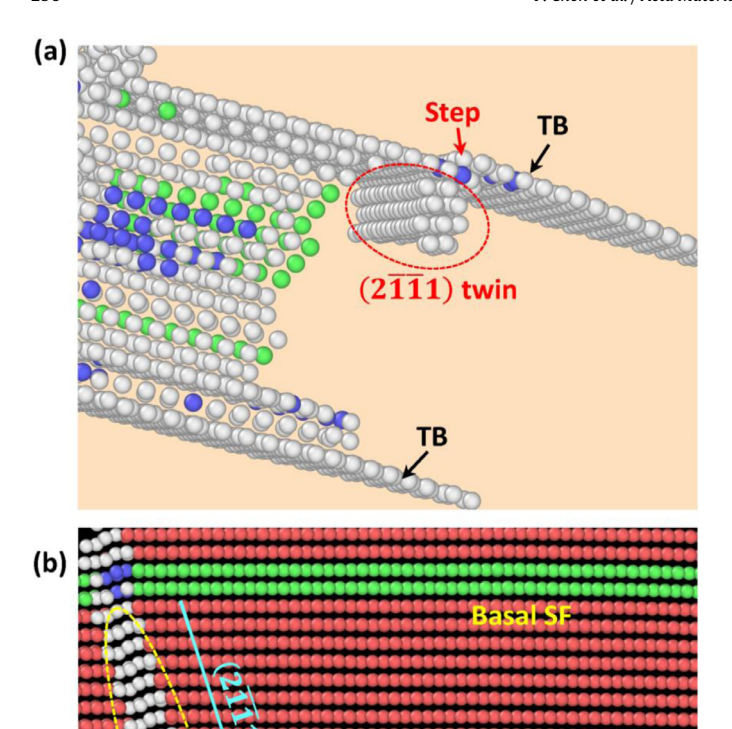


Fig. 5. (a) Side view of the $(2\overline{1}\overline{1}1)$ twin that is created by the twin-slip interaction. The twin-slip interaction creates a step at the location of impingement. (b) Tilted view of the $(2\overline{1}\overline{1}1)$ twin (the white atoms) with respect to the parent which is the $(10\overline{1}1)$ twin (the read atoms) (For interpretation of the references to color in this figure legend, the reader is referred to the web version of this article.).

(Fig. 10c). When the $(2\overline{11}1)$ twin continues transmuting to prismatic dislocations, the one-layer step grows to two layers as the $2^{\rm nd}$ dislocation exits. Meanwhile, a double layered zonal twinning dislocation is nucleated at the intersection (Fig. 10d). The Burgers vector of this twinning dislocation equals $b_{\rm T} = \frac{4\gamma^2 - 9}{2(4\gamma^2 + 3)} \left\lceil 10\overline{12} \right\rceil$ [46]. This two-layer zonal twinning dislocation glides and thickens the twin by two layers (Fig. 9e) and evens the incoherent TB. Eventually, the two-layer step disappears, and the $(10\overline{1}1)$ TB resumes coherency (Fig. 10f). The overall reaction of the two prismatic dislocations and the twinning dislocation can be described as: $2 \times \frac{1}{3} \left\lceil \overline{1120} \right\rceil + \frac{4\gamma^2 - 9}{2(4\gamma^2 + 3)} \left\lceil 10\overline{12} \right\rceil$, which eliminates the step on the opposite TB.

Fig. 11 plots the energy evolution of the pre-selected atoms in the three regions (Figs. 4a, 4d and 6c) during twin-slip interaction. In this figure, the average potential energy of the selected atoms was plotted against the energy before interaction. The X axis is the simulation time relative to a simulation timestep before the twin-slip interaction. Three energy profiles in red, green and blue are plotted in Fig. 11, corresponding to the energy of region 1, 2 and 3, respectively.

The red profile in Fig. 11 represents the interaction energy between the incoming prismatic dislocations and $(10\overline{1}1)$ TB. As the first prismatic dislocation impinges on the TB (Fig. 4a), a sharp increase in the energy occurs. The twin-slip interaction results in the nucleation of the $(2\overline{11}1)$ twin at the intersection (Fig. 4d), leading to an energy plateau on the energy plot. It can be estimated that the energy barrier for the dislocation \rightarrow twin transmutation is ~24 meV/atom. As the tensile strain further increases, another sharp

increase in the energy occurs, and this corresponds to the impingement of the $2^{\rm nd}$ prismatic dislocation on the TB at the same location (Figs. 6a and 7b). The second prismatic dislocation adds ~15.5 meV/atom on top of the ~24 meV/atom from the first prismatic dislocation. Compared to the energy barrier (~4.2 meV/atom) for $\{10\overline{1}2\}$ twinslip interaction [18], this energy barrier for interaction between ($10\overline{1}$ 1) twin and prismatic dislocations is much higher, indicating that $\{10\overline{1}1\}$ twins may be a more effective barrier to dislocation slip. This is consistent with the experimental observation by Kalidindi et al. [31] who showed $\{10\overline{1}1\}$ twins can significantly contribute to strain hardening. When the $(2\overline{1}\overline{1}1)$ twin reaches the opposite TB, the energy drops and levels out. After the $(2\overline{1}\overline{1}1)$ twin detaches from the TB where it nucleates and eventually disappears, the energy returns to the level close to before interaction.

The blue curve in Fig. 11 corresponds to the time period from the formation to disappearance of the $(2\overline{11}1)$ twin inside the $(10\overline{1}1)$ twin. A sharp increase in the energy barrier can be seen when the $(2\overline{11}1)$ twin starts forming, followed by a plateau representing the growth of $(2\overline{11}1)$ twin. As the 2nd prismatic dislocation impinges on the TB, another sharp increase in energy occurs. Then the energy levels out at about 6 meV higher than the first plateau, which is due to the interaction between the 2^{nd} prismatic dislocation and the TB. After the $(2\overline{11}1)$ twin disappears, the energy of the selected atoms drops.

The green curve in Fig. 11 shows the energy evolution of region 3, which results from the impingement of $(2\overline{11}1)$ twin on the opposite TB and the transmutation of $(2\overline{11}1)$ twin to prismatic dislocations. It can be seen that the energy barrier of the twin \rightarrow dislocation transformation is ~21 meV/atom. Therefore, the barriers of the unusual dislocation \rightarrow twin \rightarrow dislocation transmutations (Figs. 4, 6 and 7) is much higher than that of $\{10\overline{12}\}$ twin-slip interaction [18].

4. Analysis and discussion

4.1. Lattice correspondence analyses

The simulation results in this work present a very interesting but astonishing scenario in which a prismatic dislocation in the matrix is transmuted into a $(2\overline{11}1)$ twin when it impinges and interacts with a $(10\overline{1}1)$ TB, and then the $\{11\overline{2}1\}$ twin is transmuted back to prismatic dislocations at the opposite $(10\overline{1}1)$ TB. The net effect of this twin-slip interaction is that the prismatic dislocations transmit across the $(10\overline{1}1)$ twin which is a physical barrier to dislocation glide. During the interaction, the incident prismatic dislocations lose their dislocation identity by transmuting into a $(2\overline{11}1)$ twin which serves as an intermediate structure. Then the dislocation identity is resumed after the $(2\overline{11}1)$ twin is transmuted reversely to prismatic dislocations. This behavior has not been reported before. To understand the mechanism for such an unusual twin-slip interaction, in the following, a detailed analysis is conducted inside the framework of classical twinning theory.

Conceivably, the observed transformation can be understood from the perspective of lattice correspondence which is a key feature in the classical theory of deformation twinning [46]. Naturally, our analysis begins with analyzing the lattice correspondence for $\{10\overline{1}1\}$ twinning. According to Christian [46], during deformation twinning or phase transformation, there exists a uniquely defined one-to-one lattice correspondence between the parent and the twin lattice. The parent lattice is transformed to the twin lattice and this lattice transformation is achieved by a homogeneous simple shear on the twinning plane, i.e. the first invariant plane (K_1), along the twinning direction (η_1). For hcp metals, the simple shear is mediated by zonal twinning dislocations [28,46]. The lattice correspondence can be expressed by a linear transformation [46]:

$$v = Su$$
 (1)

Thus, a vector u of the parent is transformed to a vector v of the twin. These two vectors are called corresponding vectors, and S is a

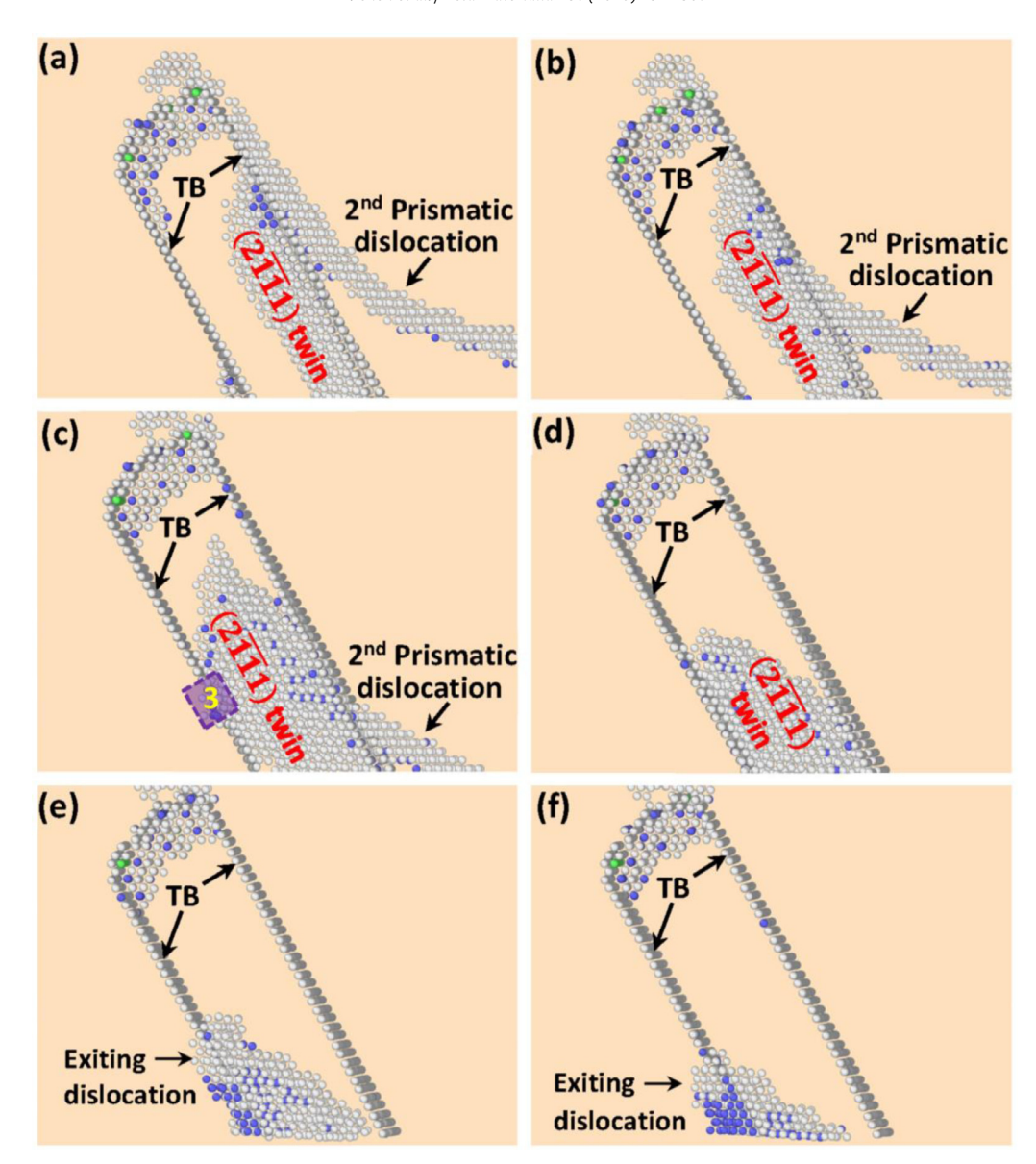


Fig. 6. (a) A second prismatic dislocation nucleates and glides on the same slip plane of the first one and interacts with the TB at the same location. (b) The top portion of the 2nd prismatic dislocation interacts with the TB, causing the $(2\overline{1}\overline{1}1)$ twin to further grow inside the $(10\overline{1}1)$ twin. (c) As the 2nd prismatic dislocation continues interacting with the $(10\overline{1}1)$ twin, the $(2\overline{1}\overline{1}1)$ twin grows and reaches the opposite $(10\overline{1}1)$ TB. A boxed region at the opposite TB was selected to compute the energy evolution as the $(2\overline{1}\overline{1}1)$ twin interacts with the opposite TB. (d) As the second prismatic dislocation completes its interaction with the $(10\overline{1}1)$ twin, the $(2\overline{1}\overline{1}1)$ twin is detaching from the $(10\overline{1}1)$ TB on the right. (e) The $(2\overline{1}\overline{1}1)$ twin is disappearing inside the $(10\overline{1}1)$ twin by forming an exiting dislocation at the $(10\overline{1}1)$ TB on the left. (f) The $(2\overline{1}\overline{1}1)$ twin eventually disappears totally.

second rank tensor. It also holds that a crystallographic plane of the parent must be transformed to a corresponding plane of the twin [47]. Using the concept of lattice correspondence, Basinski et al. [48] explained why the hardness of a twin became higher than the matrix after twinning in copper, as a result that mobile dislocations in the matrix were transmuted to immobile dislocations in the twin.

The concept of lattice correspondence in $\{10\overline{1}1\}$ twinning is graphically explained in Fig. 12 in which the parent and the twin are colored in red and green, respectively. The zone axis is along the $(1\overline{2}10)$ direction. The twinning plane or the first invariant plane, i.e., the K_1 plane, is colored in white and denoted by the blue dashed line. The red and green rectangles denote the unit cells in the parent and twin. The mirror symmetry about the twinning plane can be seen from these two unit cells. To the left, the second invariant plane, i.e. the K_2 plane $\{10\overline{13}\}_P$ (denoted by the brown line) is transformed to the K_2' plane $\{10\overline{13}\}_T$ (denoted by the green line) by the twinning shear (denoted by the blue arrow). According to the classical twinning theory [46], each crystallographic plane of the parent must

undergo exactly the same simple shear. For one example, the atoms on the parent basal plane (0002)_P (denoted by the single brown line) are sheared to the positions in the twin by the same magnitude of twinning shear (denoted by the blue arrow at the top). It can be seen that these positions are on the $\{10\overline{11}\}_T$ plane of the twin (denoted by the double green lines). Thus, this lattice transformation can be described as: $(0002)_p \rightarrow \{10\overline{11}\}_T$. Because the $\{10\overline{11}\}_T$ plane has a double-layered structure, atomic shuffles must be involved during lattice transformation. For another example, the atoms on the double-layered $\{10\overline{11}\}_p$ plane (denoted by the double brown lines) are sheared to the twin positions by the same magnitude of twinning shear as denoted by the blue arrow at the top. These twin positions are on the $(0002)_T$ plane (denoted by the single green line). Thus, this lattice transformation can be described as: $\{10\overline{11}\}_{P} \rightarrow (0002)_{T}$. Fig. 12 only shows how two crystallographic planes of the parent are transformed to the corresponding planes of the twin. Any other atomic planes must be transformed to the corresponding planes of the twin by the same twinning shear.

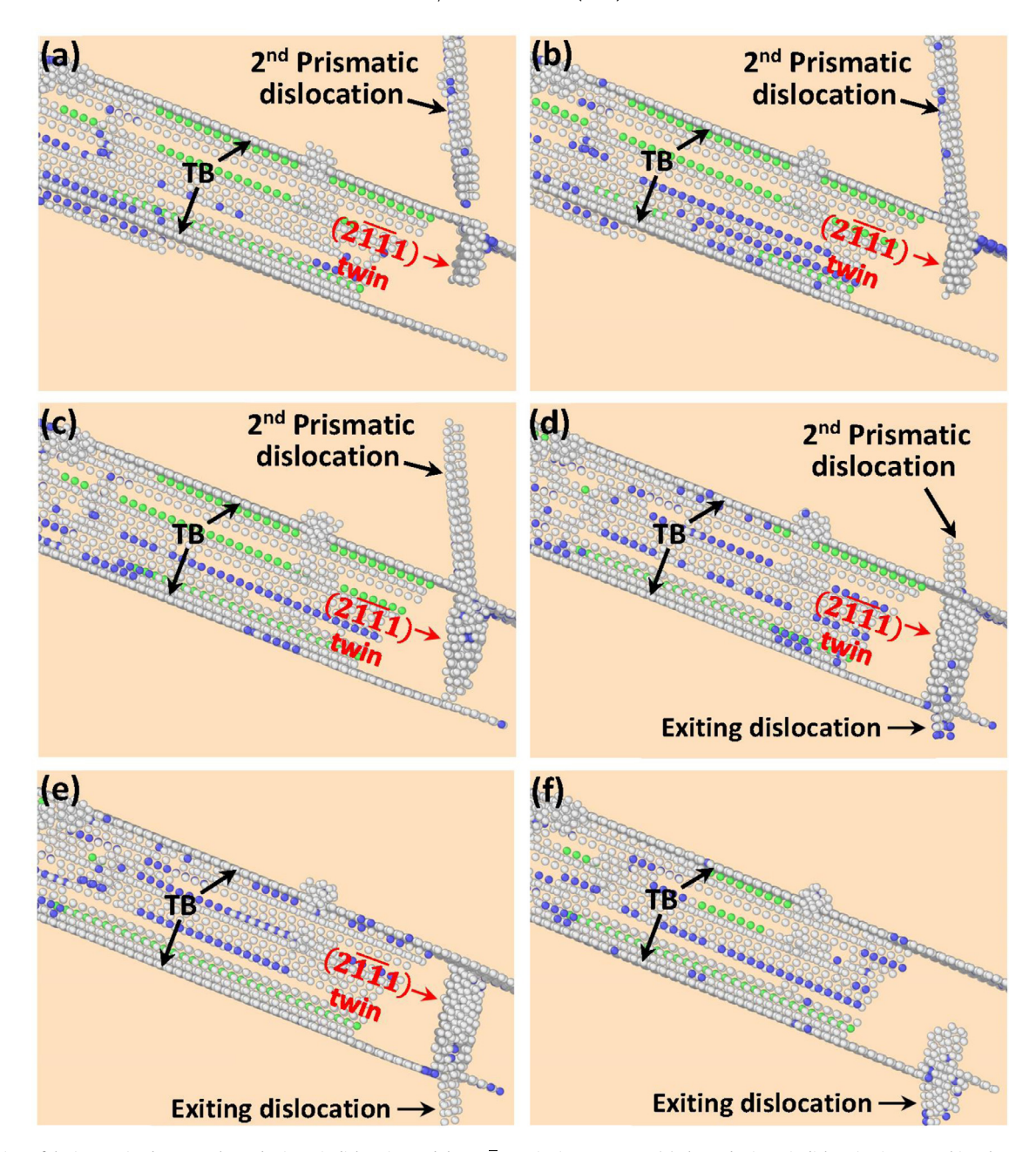


Fig. 7. Side view of the interaction between the 2nd prismatic dislocation and the $(10\overline{1}1)$ TB in time sequence. (a) The 2nd prismatic dislocation is approaching the TB at the location where the $(2\overline{1}\overline{1}1)$ twin is formed. (b) The 2nd prismatic dislocation impinges on the TB. (c) The twin-slip interaction causes the $(2\overline{1}\overline{1}1)$ twin to thicken and grow toward the opposite $(10\overline{1}1)$ TB. (d) The $(2\overline{1}\overline{1}1)$ twin reaches the opposite TB. An exiting dislocation is formed at the TB. (e) The twin-slip interaction is completed and the exiting dislocation is gliding away from the $(10\overline{1}1)$ TB. (f) The $(2\overline{1}\overline{1}1)$ twin gradually disappears from the inside of the $(10\overline{1}1)$ twin as the exiting dislocation is gliding away.

In the simulations of the current work, prismatic slip is activated, and the prismatic dislocations are transformed to a $(2\overline{11}1)$ twin inside the $(10\overline{1}1)$ twin when the prismatic dislocations are interacting with the $(10\overline{1}1)$ TB. Thus, it is necessary to analyze all the possible transformations of the prismatic planes of the parent to what planes of the twin during $(10\overline{1}1)$ twinning. To this end, another simulation was conducted with exactly the same configuration to Fig. 1a. In this simulation, three different prismatic planes and the Burgers vectors of $\langle a \rangle$ dislocations on these planes were pre-selected and tracked during deformation. Fig. 13a shows the simulation strategy. Before the simulation started, the double-layered $(1\overline{1}00)$, $(10\overline{1}0)$ and $(0\overline{1}10)$ planes were colored in pink, white and blue, respectively. Three columns of atoms along the $\langle 2\overline{1}\overline{1}0 \rangle$, i.e. the Burgers vectors of the $\langle a \rangle$ prismatic dislocations were also pre-selected and colored in purple, yellow and green, respectively. As such, the lattice transformations

involving these prismatic planes and the Burgers vectors can be tracked throughout the simulation and the transformation results can be analyzed with clarity. A tensile load was also applied along the $[\overline{2}\,110]$ direction. In Fig. 13b, a 3D view of the colored prismatic planes and the Burgers vectors are displayed and those atoms that were not pre-selected are hidden. After $(10\overline{1}\,1)$ twinning, as shown in Fig. 14, the pre-selected and pre-colored prismatic planes and Burgers vectors in the parent have been transformed to the corresponding planes and vectors in the twin. In the following, the crystallographic characteristics of the corresponding planes and vectors are analyzed carefully and in great detail.

In Fig. 15, the lattice transformation of the $(1\overline{1}00)$ prismatic plane and the $[\overline{11}20]$ vector after $(10\overline{1}1)$ contraction twinning is analyzed. In Fig. 15a, the twin lattice is tilted such that the transformed pink plane is edge-on, whereas the blue and white plane are inclined. In

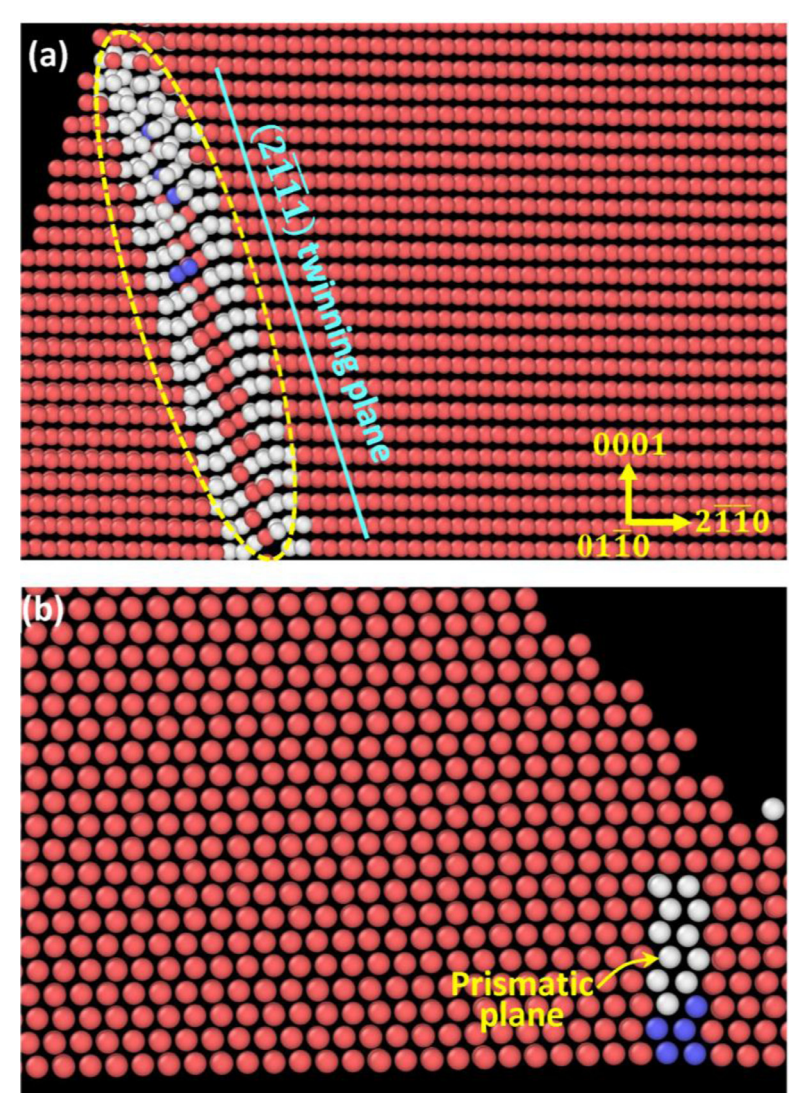


Fig. 8. (a) A close-up of the ($2\overline{1}\overline{1}$) twin created by the twin-slip interaction. (b) The exiting dislocation is a prismatic dislocation in the matrix which has the same Burgers vector of the incoming prismatic dislocations in Figure 4, 6-7.

this plot, only a thin slice of the bulk is shown. Next, the boxed region in Fig. 15a is magnified and analyzed in Fig. 15b. It can be seen that the pink atoms lie on four consecutive $(2\overline{111})$ planes, indicating that the parent $(1\overline{1}00)$ prismatic plane has been transformed to the $(2\overline{1}\overline{1}1)$ plane in the twin. Note this is the twinning plane of the twin inside the $(10\overline{1}1)$ twin. The purple atoms appear to be parallel to the ($2\overline{11}$ 1) plane after transformation, however, the direction of the purple atoms cannot be determined in this view. To determine the direction along which the purple atoms are aligned, as shown in Fig. 15c, we tilt the view of Fig. 15b to another viewing direction. In this plot, it can be seen that the purple atoms also lie in the $(0\overline{1}11)$ plane. Thus, the purple atoms must be at the intersection of the $(0\overline{1}11)$ plane and the $(2\overline{1}\overline{1}1)$ plane. In Fig. 15d, the $\langle c \rangle$ component of the transformed vector is analyzed. The viewing direction is along the $[0\overline{1}10]$ direction and three atoms 1, 2 and 3 are highlighted. The distance between atom 1 and 2 along the [0001] equals $\langle c \rangle$. Then, we tilt Fig. 15d such that the viewing direction is along the [0001] to determine the $\langle a \rangle$ component of the transformed vector (Fig. 15e). Atom 1, 2 and 3 are on every other basal planes. The projected distance from atom 1 to atom 2 on basal plane is a full $\langle a \rangle$, i.e., $\frac{1}{3}[\overline{1}2\overline{1}0]$. It is now clear that, the $\langle a \rangle = \frac{1}{3} [\overline{1120}]$ vector in the parent is transformed to a $\langle c + a \rangle$, i.e., $[0001] + \frac{1}{3}[\overline{1}2\overline{1}0] = \frac{1}{3}[\overline{1}2\overline{1}3]$, by the $(10\overline{1}1)$ twinning. These analyses are schematically shown in Fig. 15f. The purple plane is the $(2\overline{1}\overline{1}1)$ that is transformed from the parent $(1\overline{1}00)$, and the purple atoms are along the $\frac{1}{3}[\overline{1}2\overline{1}3]$ in the $(10\overline{1}1)$ twin. The $\frac{1}{3}[\overline{1}2\overline{1}3]$ is at the intersection of the $(0\overline{1}11)$ and $(2\overline{1}\overline{1}1)$. Hence, during $(10\overline{1}1)$ twinning, the lattice transformation for the prismatic plane and the Burgers vector in the matrix can be described as:

$$\left(1\overline{1}00\right)\left[\overline{1}\overline{1}20\right]_{\textit{Parent}} \rightarrow \left(2\overline{1}\overline{1}1\right)\left[\overline{1}2\overline{1}3\right]_{\textit{Twin}} \tag{2}$$

Next, we perform similar analysis for lattice transformation of the $(10\overline{1}\,0)$ prismatic plane and $\frac{1}{3}[\overline{1}2\overline{1}0]$ Burgers vector by the $(10\overline{1}\,1)$ twinning. The results are shown in Fig. 16. First, the twin lattice is tilted such that the white plane is edge-on (Fig. 16a). In this thin slice, the pink and blue plane are inclined. Then the boxed region in Fig. 16a is magnified and analyzed (Fig. 16b). It is clear that the white atoms are located on two consecutive $(10\overline{1}\,3)$ planes in the twin, indicating the parent $(10\overline{1}\,0)$ prismatic plane is transformed to the $(10\overline{1}\,3)$ in the twin. In addition, the yellow atoms are parallel to the viewing direction, i.e., along the $[\overline{1}\,2\overline{1}\,0]$. Thus, the Burgers vector remains unchanged before and after twinning. Notably, this vector is also parallel to the zone axis of the $(10\overline{1}\,1)$ twins, i.e. $[\overline{1}\,2\overline{1}\,0]$. Hence, the above transformation can be described as:

$$\left(10\overline{1}0\right) \left[\overline{1}2\overline{1}0\right]_{Parent} \rightarrow \left(10\overline{1}3\right) \\ \left[\overline{1}2\overline{1}0\right]_{Twin}$$
 (3)

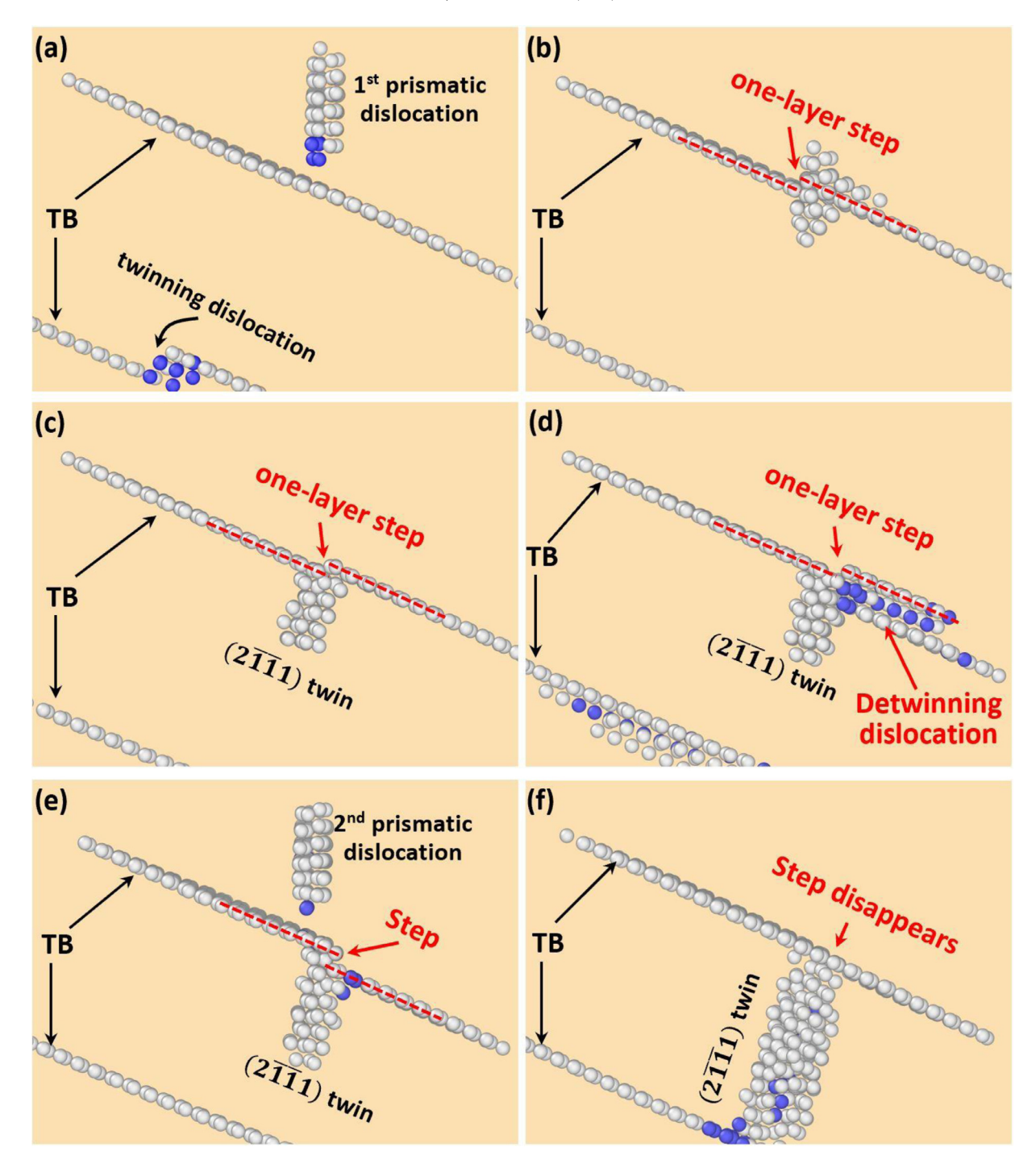


Fig. 9. Evolution of the steps at the $(10\overline{1}1)$ TB when the matrix prismatic dislocations interact with the TB. (a) The 1st prismatic dislocation is approaching the coherent TB. (b) A one-layer step is generated at the TB when the dislocation is interacting with the TB. (c) The one-layer step and the $(2\overline{1}\overline{1}1)$ twin can be seen. (d) A double layered detwinning dislocation glides toward the step and shrinks the twin by two $(10\overline{1}1)$ planes. (e) After detwinning, the step swaps side. The 2nd prismatic dislocation is approaching the TB. (f) The $(10\overline{1}1)$ TB resumes coherency after interaction with the 2nd prismatic dislocation.

The lattice transformation of the $(0\overline{1}10)$ prismatic plane and $\frac{1}{3}[2\overline{1}\overline{1}0]$ Burgers vector by the $(10\overline{1}1)$ twinning is also analyzed similarly and the results are shown in Fig. 17. First, as shown in Fig. 17a, the $(10\overline{1}1)$ twin is tilted such that the blue plane is edge-on, whereas the pink and the white planes are inclined. Then the boxed region in Fig. 17a is magnified and analyzed (Fig. 17b). It can be seen that after twinning, all the blue atoms are located on a corrugated $(1\overline{1}01)$ plane, and the green atoms are parallel to the $(1\overline{1}01)$. When the box is tilted to another zone axis $[1\overline{2}10]$, it can be found that the green atoms are also parallel to the $(\overline{1}011)$ plane. Thus, the green atoms, which

represent the vector transformed from the original $\langle a \rangle = \frac{1}{3}[2\overline{11}0]$, actually lie at the intersection of the $(\overline{1}011)$ and $(1\overline{1}01)$ planes (Fig. 17c). To determine the $\langle c \rangle$ component of the transformed vector along the green atoms, the box is tilted to the zone axis of $[11\overline{2}0]$, as shown in Fig. 17d. Five green atoms are selected and numbered. Atoms 1, 3 and 5 are along exactly the same line while atoms 2 and 4 are on the corrugated positions but along the same direction as are atoms 1, 3 and 5. It can be seen that the distance from atom 1 to atom 3 along the [0001] is a full $\langle c \rangle$. After the box is tilted to the [0001] view direction, the basal component of the transformed vector can

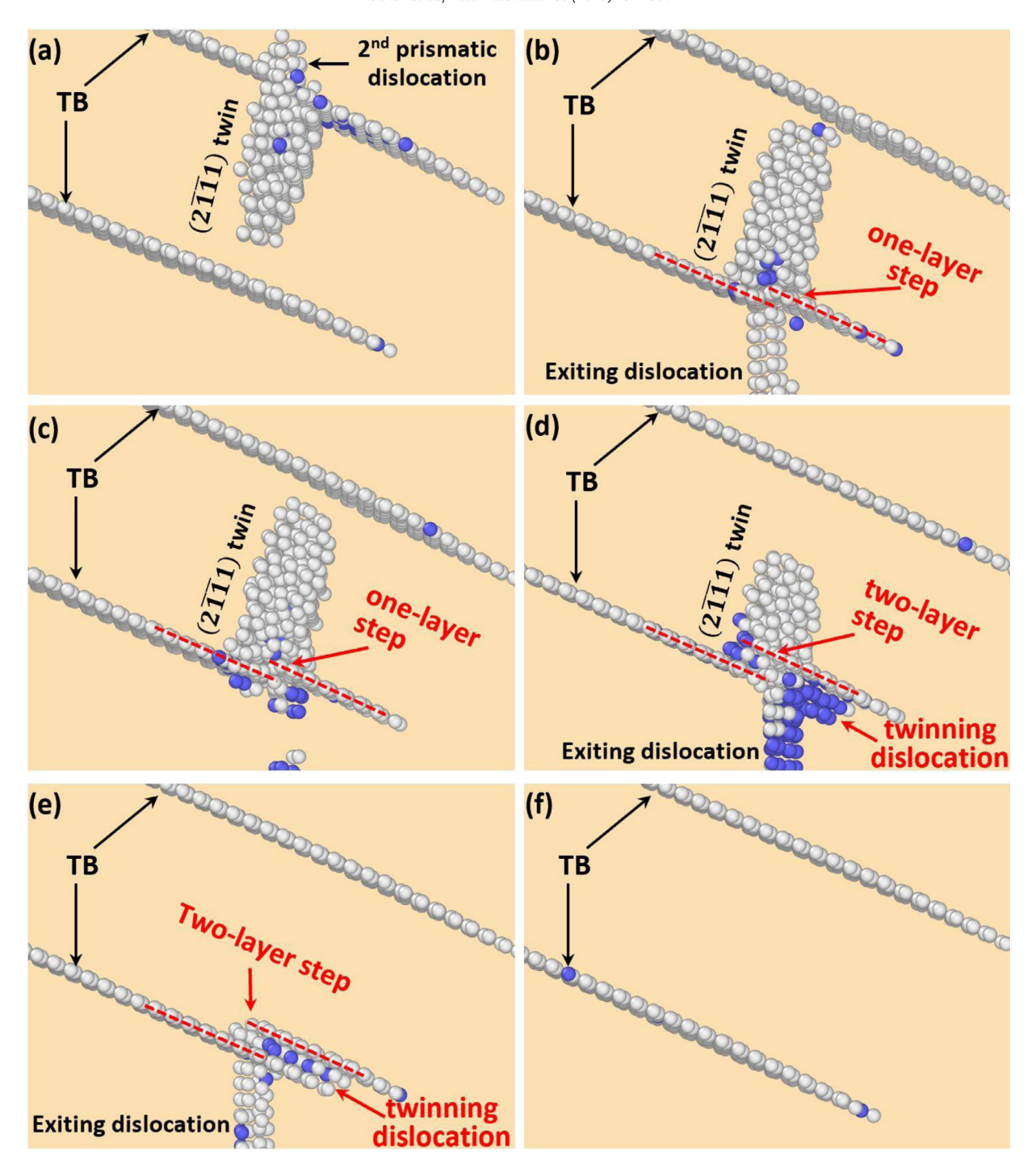


Fig. 10. Evolution of the step at the $(10\overline{1}1)$ TB as the $(2\overline{1}\overline{1}1)$ twin is transmuted back to prismatic dislocations in the parent. (a) The $(2\overline{1}\overline{1}1)$ twin is approaching the coherent $(10\overline{1}1)$ TB. (b) A one-layer step is generated at the TB as the $(2\overline{1}\overline{1}1)$ twin is transmuted into a prismatic dislocation in the parent. (c) A one-layer step is left at $(10\overline{1}1)$ TB after the first dislocation exits. (d) The $(2\overline{1}\overline{1}1)$ twin is transmuted into a 2nd prismatic dislocation. The step height increases to two layers. Meanwhile, a twinning dislocation is being nucleated at the intersection. (e) The twinning dislocation glides and thickens the $(10\overline{1}1)$ twin by two layers and removes the two-layer step (f).

be determined as $[01\overline{1}0]$, as shown in Fig. 17e. Thus, the $\frac{1}{3}[2\overline{11}0]$ vector in the parent is transformed to $[0001]+[01\overline{1}0]=[01\overline{1}1]$ by the $(10\overline{1}1)$ twinning. These analyses are crystallographically summarized in Fig. 17f. The shaded blue plane is the $(1\overline{1}01)$ which is transformed from the parent $(0\overline{1}10)$. The green atoms are along the green vector of $[01\overline{1}1]$ in the $(10\overline{1}1)$ twin. This transformed vector is at the intersection of the $(\overline{1}011)$ and $(1\overline{1}01)$. Thus, the lattice transformation can be described as:

$$\left(0\overline{1}10\right)\left[2\overline{1}\overline{1}0\right]_{\textit{Parent}} \rightarrow \left(1\overline{1}01\right)\left[01\overline{1}1\right]_{\textit{Twin}} \tag{4}$$

Following the pioneer works of Christian and Basinski [46,48], Niewczas [49] developed the lattice correspondence matrices for all four major twinning modes of HCP metals. Transformations of some crystallographic planes and directions by the twinning modes in Mg and Ti were calculated. In the case of $\{10\overline{1}1\}$ $(10\overline{12})$ twinning mode in Mg [49], the lattice correspondence of the basal, prismatic and pyramidal slip systems were provided. In Table 1, the calculated results for the prismatic plane by Niewczas [49] and the results obtained by our atomistic simulations were listed and compared.

From Table 1, consistency and discrepancy between the mathematical calculations [49] and our simulations can be seen. For the

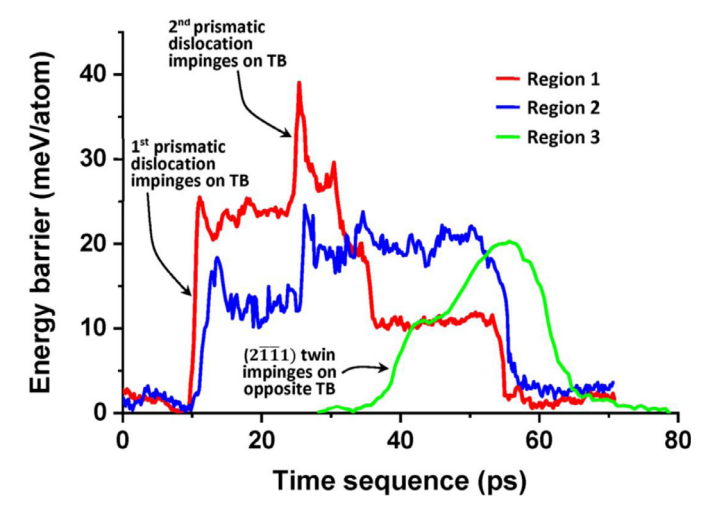


Fig. 11. Evolution of the selected atoms (region 1, 2 and 3 in Figs. 4 and 6) during twinslip interaction. The red curve is the energy evolution of region 1 (Fig. 4a), corresponding to the interaction between the incoming prismatic dislocations and $(10\overline{1}\,1)$ TB. The blue curve represents the energy evolution of region 2 (Figure 4d), which corresponds to the formation and disappearance of the $(2\overline{1}\,\overline{1}\,1)$ twin inside $(10\overline{1}\,1)$ twin. The green curve is the energy evolution of region 3 (Fig. 6c), corresponding to the processes of $(2\overline{1}\,\overline{1}\,1)$ twin impinging on the opposite TB and then transforming to the prismatic dislocations (For interpretation of the references to color in this figure legend, the reader is referred to the web version of this article.).

 $(10\overline{1}0)$ $[\overline{1}2\overline{1}0]$ slip system, the agreement is excellent. Thus, crystallographically, this prismatic slip system would be transformed to a slip system on the $(10\overline{1}3)$ plane in the twin while retaining the original Burgers vector, which is also the zone axis of the twins. For the $(0\overline{1}10)[2\overline{1}\overline{1}0]$ slip system, our results show that, this $(0\overline{1}10)$ prismatic plane should be transformed to the $(1\overline{1}01)$ pyramidal plane and the Burgers vector should be transformed to the $[01\overline{1}1]$. If we compare our simulation result with the calculated result, a discrepancy can be seen but the difference between these results is insignificant. For example, the $(1\overline{4}3\overline{3})$ in the table is very close to the $(0\overline{1}1\overline{1})$, and the $[\overline{5}41\overline{6}]$ is very close to the $[\overline{1}10\overline{1}]$. Thus, most likely, the round-off error in the

matrix transformation is responsible for the discrepancy. A more significant discrepancy can be found in the case of $(1\overline{1}00)[\overline{1}\overline{1}20]$. Our results show that the $(1\overline{1}00)$ prismatic plane should be transformed to the $(2\overline{1}\overline{1}1)$ pyramidal plane and the Burgers vector $[\overline{1}\overline{1}20]$ should be transformed to the $[\overline{1}2\overline{1}3]$ in the twin, but the calculated result shows that the transformed plane is the $(\overline{3}4\overline{1}\overline{3})$ and the transformed direction is the $[14\overline{5}6]$.

4.2. Mechanism for the dislocation \rightarrow twin \rightarrow dislocation transformations

Based on the lattice correspondence analyses, it can now be understood why a gliding prismatic dislocation in the matrix can be transformed into a $(2\overline{11}1)$ twin inside a $(10\overline{1}1)$ twin when interacting with the coherent $(10\overline{1}1)$ TBs.

As seen in Fig. 4, a $(1\overline{1}00)\frac{1}{3}[\overline{11}20]$ prismatic dislocation in the matrix interacts with a $(10\overline{1}1)$ TB and the matrix dislocation is transformed to a $(2\overline{11}1)$ twin with a thickness of a couple of atomic layer inside the $(10\overline{1}1)$ twin. As analyzed in Fig. 15, the slip plane of the matrix prismatic dislocation, i.e. $(1\overline{1}00)$, is transformed to the $(2\overline{11}1)$ plane of the $(10\overline{1}1)$ twin and this $(2\overline{11}1)$ plane is exactly one of the twinning planes of HCP metals although not a slip plane. The Burgers vector of the prismatic dislocation in the matrix, i.e. $\frac{1}{3}[\overline{11}20]$ is transformed to the $[\overline{12}\overline{13}]$ of the $(10\overline{1}1)$ twin. But the Burgers vector of the twinning dislocations of $\{11\overline{2}1\}$ twinning should be along the $(11\overline{26})$. According to Vaidya and Mahajan [50], formation of a zonal twinning dislocation for $\{11\overline{2}1\}$ twinning can be described with the following dislocation reaction:

$$\frac{1}{3} \left\langle \overline{1} 2 \overline{1} 3 \right\rangle = \frac{1}{2} \cdot \frac{1}{3} \left\langle \overline{2} 116 \right\rangle + \frac{1}{2} \left\langle 01 \overline{1} 0 \right\rangle \tag{5}$$

Thus, the twinning Burgers vector is a major component of the transformed vector $[\overline{12}\overline{13}]$, although the transformed vector in theory is not exactly along the direction of twinning shear. The transformations of the slip plane and the Burgers vector of a prismatic dislocation in the matrix make possible the dislocation \rightarrow twin \rightarrow dislocation transformation, at least crystallographically such an interesting transformation is feasible.

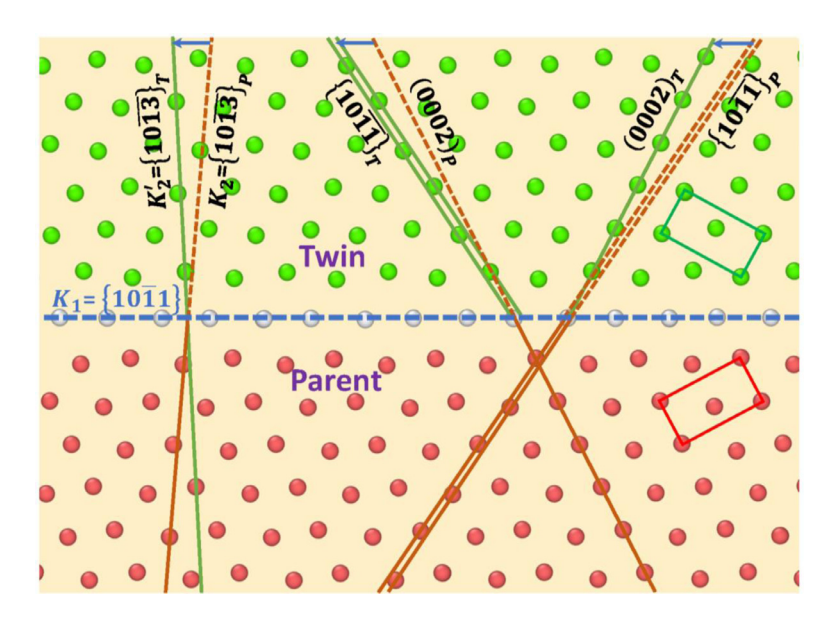


Fig. 12. Illustration of lattice correspondence in $\{10\overline{1}1\}$ ($10\overline{12}$) twinning. The parent and the twin are colored in red and green, respectively. Zone axis ($1\overline{2}10$). The twinning plane, i.e., the K_1 plane, is colored in white and denoted by blue dashed line. To the left, the K_2 plane $\{10\overline{13}\}_P$ (denoted by the brown line) is transformed to the K_2 plane $\{10\overline{13}\}_T$ (denoted by the green line) by the twinning shear (denoted by the blue arrow). Because each plane of the parent must undergo exactly the same twinning shear, as a result, the parent (0002) $_P$ plane (denoted by the single brown line) is transformed to the twin $\{10\overline{11}\}_T$ plane (denoted by the double green lines). Similarly, the parent $\{10\overline{11}\}_P$ plane (denoted by the double brown lines) is transformed to the twin $(0002)_T$ (denoted by the single green line). The rectangles denote the lattice units in the parent and twin to show the mirror symmetry (For interpretation of the references to color in this figure legend, the reader is referred to the web version of this article.).

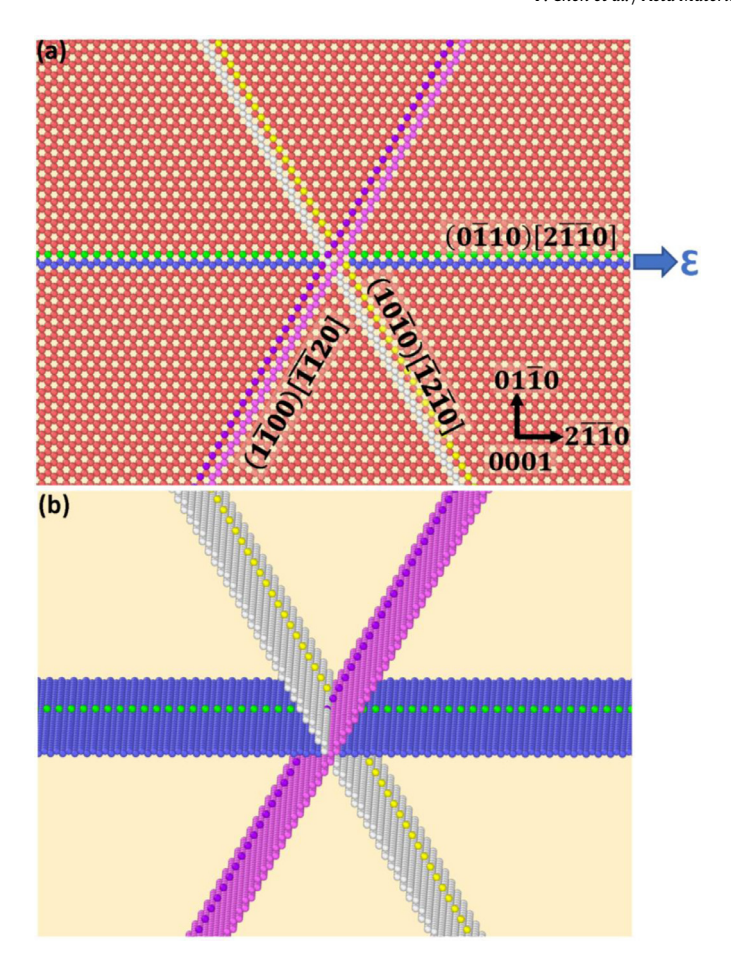


Fig. 13. To analyze the lattice transformation during twin-slip interaction, another simulation was conducted with a similar configuration to Fig. 1a but three different prismatic planes and the Burgers vectors of $\langle a \rangle$ prismatic dislocations were pre-selected and colored differently. (a) Before twinning, the double layered $(1\bar{1}00)$, $(10\bar{1}0)$ and $(0\bar{1}10)$ plane were colored in pink, white and blue, respectively. Three columns of atoms that are along the $(2\bar{1}\bar{1}0)$, i.e. the corresponding Burgers vectors of the prismatic dislocations were also pre-selected and colored in purple, yellow and green, respectively. (b) 3D view of the colored prismatic planes and vectors. The red atoms in the lattice are hidden (For interpretation of the references to color in this figure legend, the reader is referred to the web version of this article.).

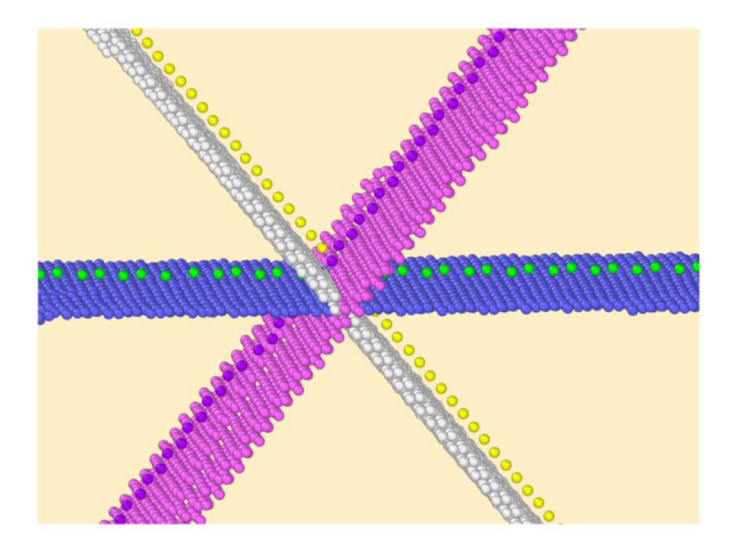


Fig. 14. After $(10\overline{1}1)$ twinning, the pre-selected and pre-colored prismatic planes and Burgers vectors in the parent are transformed to corresponding planes and vectors in the twin.

4.3. Comparison with twin-slip interaction in $\{10\overline{1}2\}$ mode

Twin-slip interaction for $\{10\overline{1}2\}$ mode has been investigated extensively by experiments and simulations [17,20,22,51], in an attempt to account for mechanical properties of Mg alloys. It was shown that only those dislocations with a Burgers vector parallel to the zone axis of $\{10\overline{1}2\}$ twins can be transmuted [18]. In stark contrast in this work, the Burgers vector of the matrix dislocation $\frac{1}{3}[\overline{11}20]$ is not parallel to the zone axis of the twins $\frac{1}{2}[\overline{1}2\overline{1}0]$ (Fig. 3), but transmutation still occurs. The product vector of the lattice transformation, i.e. $[\overline{1213}]$, is slightly away from the twinning direction. On the other hand, the transformation of the prismatic slip plane exactly follows the correspondence predicted by the classical twinning theory. Most interestingly, the mobile prismatic dislocation in the matrix was not transmuted to an immobile dislocation in the contraction twin; instead, it was transmuted to a $(2\overline{11}1)$ twin. The growth of the $(2\overline{1}\overline{1}1)$ was sustained by the transmutation of successive prismatic dislocations that impinged at the same location. After the $(2\overline{11}1)$ twin reached the opposite TB, it was transmuted back to prismatic dislocations which exited the $(10\overline{1}1)$ twin. Hence, the matrix dislocations are not absorbed by the TB despite that their Burgers vector is non-parallel to the zone axis of the twins. Similarly, the interaction of a basal dislocation with $(10\overline{1}1)$ TB is also very different from the $\{10\overline{1}2\}$ twin-basal dislocation interaction. Li et al. [35] reported that when a basal dislocation whose Burgers vector is not parallel to the zone axis of the $(\overline{1}011)$ twin, this basal dislocation can still be transmuted into a pyramidal dislocation on $(10\overline{1}1)$ plane of the twin, which is a corresponding plane of the parent basal plane. Similar lattice transformation was reported by Peng et al. [32].

The difference between twin-slip interactions for $\{10\overline{1}2\}$ extension twinning and $\{10\overline{1}1\}$ contraction twinning deserves further investigations. Herein we only provide preliminary discussion of underlying physics responsible for the difference. The twinning mechanism is very different between these two twinning modes. For $\{10\overline{1}2\}$ twinning, it has been extensively reported that TBs are highly incoherent and can hugely deviate from the twinning plane in experiments [24,39,52] and simulations [23,53]. Using molecular dynamics simulation, Li and Ma [54] found that $\{10\overline{1}2\}$ twinning is actually mediated by atomic shuffling which transforms the "parent basal to twin prismatic and parent prismatic to basal". Li and Zhang [23] further proved that the twinning shear should be zero for $\{10\overline{1}2\}$ mode because of the breakdown of the invariant plane strain condition which is a fundamental assumption in classical twinning theory. Recent reports [18,53,55] have shown that, despite the definitions of twinning disconnection [56,57] and disclination [58] on highly incoherent $\{10\overline{1}2\}$ TBs, when lattice correspondence analysis was performed, the twinning mechanism in the works claiming disconnection and disclination is exactly the same as the Li-Ma [54] shuffling mechanism. During TB migration, atomic shuffles, which are required to accomplish the lattice transformation, distort the structure of the theoretical twinning plane, leading to extremely incoherent TB structures. During interaction of incoherent TBs with incoming matrix dislocations, most of the matrix dislocations are absorbed by the TBs which act as a dislocation sink, except for those with a Burgers vector parallel to the zone axis of the twins [18]. Although some prismatic dislocations are supposed to be transformed to $\{11\overline{2}3\}$ pyramidal dislocations according to lattice correspondence calculations, such transformation does not occur possibly due to the large Burgers vector and complex core structure of pyramidal dislocations.

For {1011} twinning, Li and Ma [28] showed that this twinning mode very well follows the classical twinning theory. A twinning shear can be well defined on the twinning plane which remains coherent during TB migration and zonal twinning dislocations are involved in twin growth. Large atomic shuffles are also needed but

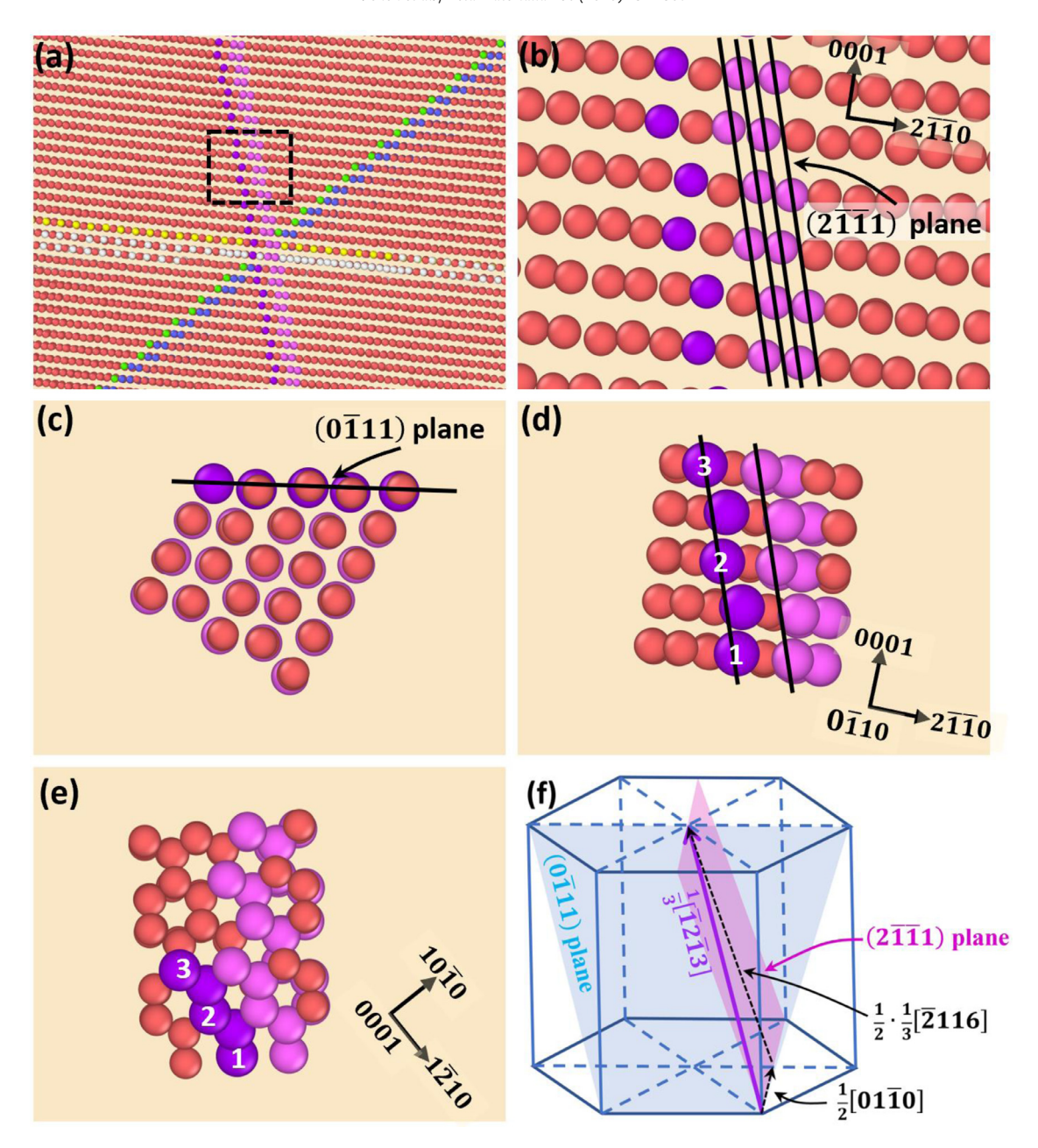


Fig. 15. Lattice correspondence analysis for the $(1\overline{1}00)$ prismatic plane and $\frac{1}{3}[\overline{1}\overline{1}20]$ Burgers vector after $(10\overline{1}1)$ twinning. (a) The twin lattice is tilted such that the transformed pink plane is edge-on, and the white and blue planes are inclined. Only a thin slice is shown. (b) Magnified view of the boxed region in (a). It can be seen that after twinning, the parent $(1\overline{1}00)$ prismatic plane is transformed to the $(2\overline{1}\overline{1}1)$ plane in the twin. The purple atoms are also parallel to the $(2\overline{1}1)$ plane of the twin. (c) Tilted view of (b) such that the purple atoms lie at the intersection of the $(0\overline{1}11)$ plane and the $(2\overline{1}\overline{1}1)$ plane. (d) The transformed Burgers vector has a (c) component. The distance between atom 1 and atom 2 along the [0001] equals (c). (e) Basal view of the purple atoms which are projected along the $\frac{1}{3}[\overline{1}2\overline{1}0]$. Thus, the $\frac{1}{3}[\overline{1}20]$ vector in the parent is transformed to (c+a), i.e., $\frac{1}{3}[\overline{1}2\overline{1}3]$, by the $(10\overline{1}1)$ twinning. (f) Crystallography of the lattice transformation. The purple plane is the $(2\overline{1}\overline{1}1)$ that is transformed from the parent $(1\overline{1}00)$, and the purple atoms the $\frac{1}{3}[\overline{1}2\overline{1}3]$ in the $(10\overline{1}1)$ twin. The $\frac{1}{3}[\overline{1}2\overline{1}3]$ is at the intersection of the $(0\overline{1}11)$ and $(2\overline{1}\overline{1}1)$ (For interpretation of the references to color in this figure legend, the reader is referred to the web version of this article.).

the shuffles are nearly along the same direction and inside the twinning plane. Thus, the twin boundaries retain the coherency during twin growth, as revealed in experiments and simulations [59]. The coherent TB structure might be an important factor determining dislocation transformation at the TBs. For example, the other two prismatic dislocations, i.e. $(0\overline{1}10)[2\overline{1}10]$ and $(10\overline{1}0)[12\overline{1}0]$ might be able to transform to defects on $\{10\overline{1}1\}$ and $\{10\overline{1}3\}$ planes, according to the lattice correspondence analyses in this work. However, more simulations are needed to verify this point. In addition, in-situ TEM experiments might be able to provide more insight from experimental observations.

5. Conclusions

In this work, interaction between matrix prismatic dislocations and $\{10\overline{1}1\}$ TBs was investigated by atomistic simulations. Very unusual dislocation \rightarrow twin \rightarrow dislocation transmutations on the TBs were observed. The following conclusions can be reached:

(1) When a matrix prismatic dislocation interacts with a $\{10\overline{1}1\}$ TB, the prismatic dislocation can be transmuted to a $\{11\overline{2}1\}$ twin inside the $\{10\overline{1}1\}$ twin. When a second matrix prismatic dislocation impinges on the TB at the same location as does the first

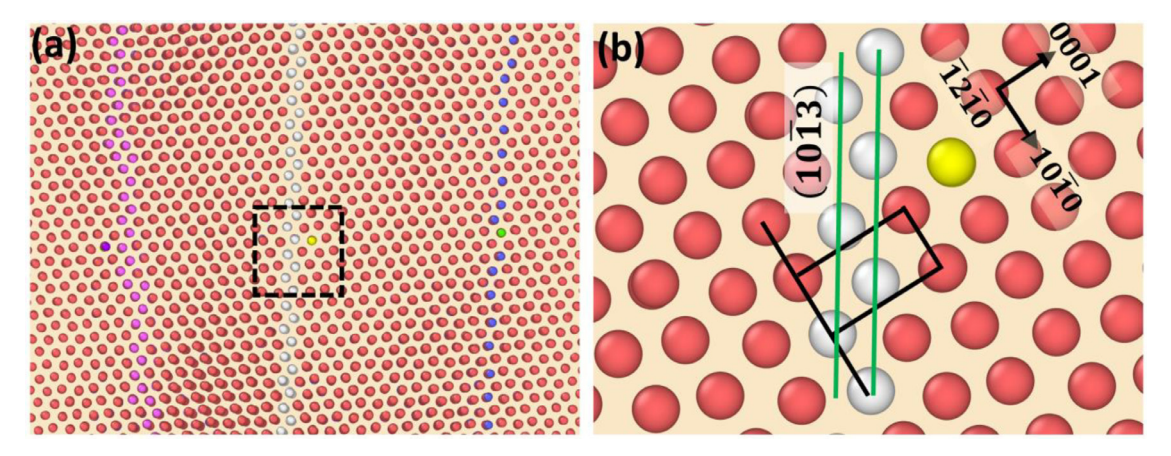


Fig. 16. Lattice correspondence analysis for the $(10\overline{1}0)$ prismatic plane and $\frac{1}{3}[\overline{1}2\overline{1}0]$ Burgers vector after $(10\overline{1}1)$ twinning. (a) The twin lattice is tilted such that the white plane is edge-on, and the pink and blue planes are inclined. Only a thin slice is shown. (b) Magnified view of the boxed region in (a). It can be seen that the after twinning, the parent $(10\overline{1}0)$ prismatic plane is transformed to the $(10\overline{1}3)$ in the twin. The yellow atoms are parallel to the viewing direction, i.e., along the $[\overline{1}2\overline{1}0]$. Thus, the Burgers vector remains unchanged before and after twinning. Notably, this vector is parallel to the zone axis of the $(10\overline{1}1)$ twins, i.e. $[\overline{1}2\overline{1}0]$ (For interpretation of the references to color in this figure legend, the reader is referred to the web version of this article.).

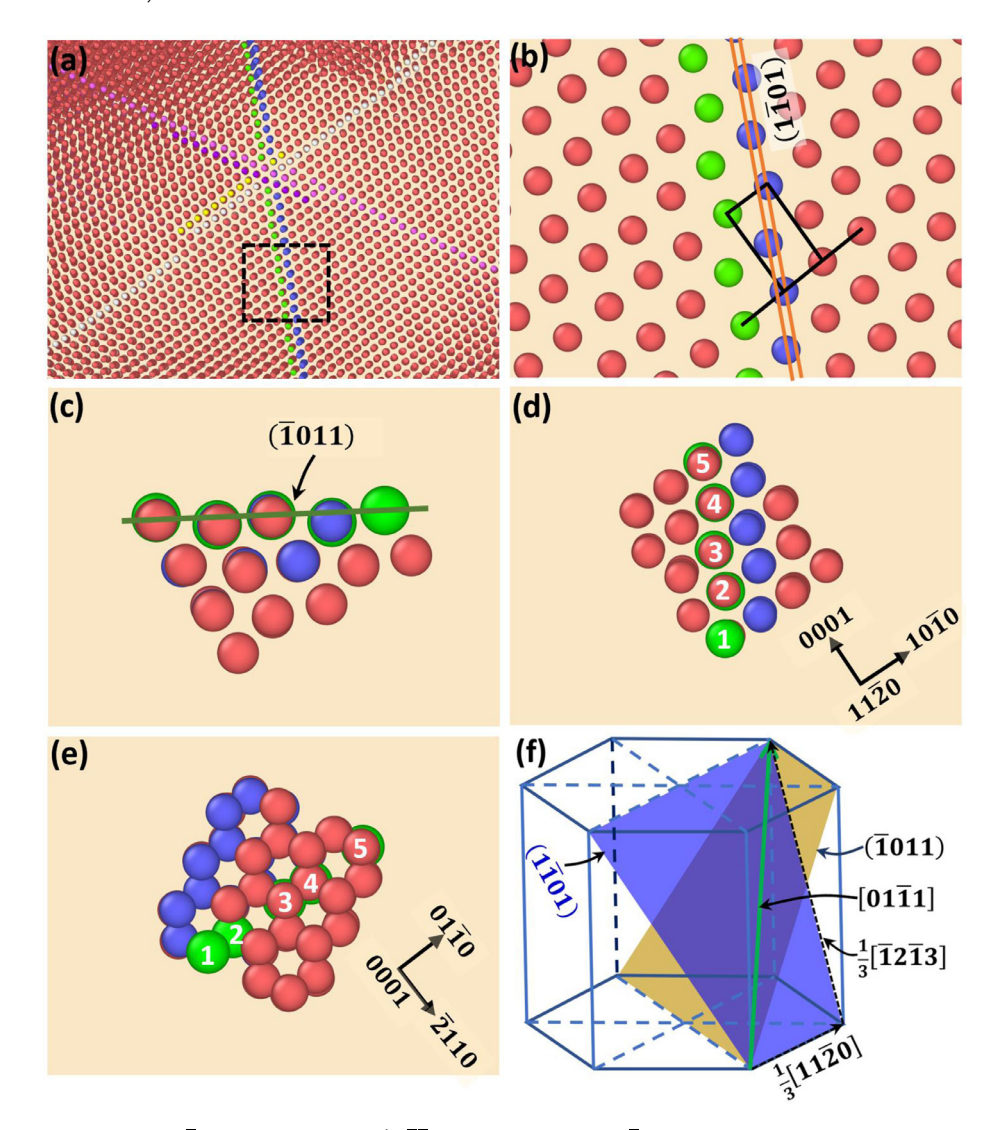


Fig. 17. Lattice correspondence analysis of the $(0\overline{1}10)$ prismatic plane and $\frac{1}{3}[2\overline{1}\overline{1}0]$ Burgers vector after $(10\overline{1}1)$ twinning. (a) The twin lattice is tilted such that the blue plane is edge-on, and the pink and white planes are inclined. Only a thin slice is shown. (b) Magnified view of the boxed region in (a). All the blue atoms are located on a corrugated $(1\overline{1}01)$. The green atoms are also parallel to the $(1\overline{1}01)$. (c) Tilted view of (b) such that the green atoms lie at the intersection of the $(\overline{1}011)$ and $(\overline{1}\overline{1}01)$. (d) The vector represented by the green atoms has a (c) component. (e) Basal view of the green atoms. It can be seen that the green atoms are projected along the $[01\overline{1}0]$ of the basal. Thus, the $\frac{1}{3}[2\overline{1}\overline{1}0]$ vector in the parent is transformed to $[001] + [01\overline{1}0] = [01\overline{1}1]$ by the $(10\overline{1}1)$ twinning. (f) Crystallography of the lattice transformation. The shaded blue $(1\overline{1}01)$ is transformed from the parent $(0\overline{1}10)$. The green atoms are along the green vector of $[01\overline{1}1]$ in the $(10\overline{1}1)$ twin. This vector is at the intersection of the $(\overline{1}011)$ and $(1\overline{1}01)$ (For interpretation of the references to color in this figure legend, the reader is referred to the web version of this article.).

Table 1 Crystallographic transformations of prismatic dislocations by $\{10\overline{1}1\}$ twinning

Slip system in matrix	Slip system in twin (this work)	Slip system in twin (by Niewczas [49])
$\begin{array}{c} (1\overline{1}00)[\overline{1}\overline{1}20] \\ (10\overline{1}0)[\overline{1}2\overline{1}0] \\ (0\overline{1}10)[2\overline{1}\overline{1}0] \end{array}$	$(2\overline{1}\overline{1}1) [\overline{1}2\overline{1}3] (10\overline{1}3)[\overline{1}2\overline{1}0] (1\overline{1}01)[01\overline{1}1]$	$(\overline{3}4\overline{13})[14\overline{5}6]$ $(10\overline{13})[1\overline{2}10]$ $(1\overline{4}3\overline{3})[541\overline{6}]$

- dislocation, the $\{11\overline{2}1\}$ twin grows toward the opposite $\{10\overline{1}1\}$ TB. Thus, the matrix prismatic dislocations lose their identity after transformation at the $\{10\overline{1}1\}$ TB.
- (2) The $\{11\overline{2}1\}$ twin transforms back to prismatic dislocations when the twin front reaches the opposite $\{10\overline{1}1\}$ TB. The transformed prismatic dislocations exit the $\{10\overline{1}1\}$ twin and glide into the matrix. As such, the prismatic dislocations resume their dislocation identity and the net effect of the interaction between the matrix prismatic dislocations and $\{10\overline{1}1\}$ twin is that the matrix prismatic dislocations transmit across the $\{10\overline{1}1\}$.
- (3) The dislocation→twin→dislocation transmutations can be well understood from the perspective of lattice correspondence which requires that a crystallographic plane of parent must be transformed into a corresponding plane of twin. The slip plane of the matrix prismatic dislocation is transformed into a {1121} which is a twinning plane.
- (4) Lattice transformation for the other two prismatic planes were calculated in our simulation and the results show consistency and discrepancy between the atomistic simulations and the crystallography-based calculations. Analyses from atomistic simulation are more reliable.

Declaration of Competing Interest

The authors declare that they have no known competing financial interests or personal relationships that could have appeared to influence the work reported in this paper.

Acknowledgements

Bin Li gratefully thanks the support from the U.S. National Science Foundation (NSF) (CMMI-1635088).

References

- X. Li, Y. Wei, L. Lu, K. Lu, H. Gao, Dislocation nucleation governed softening and maximum strength in nano-twinned metals, Nature 464 (2010) 877–880, doi: 10.1038/nature08929.
- [2] T. Ezaz, M.D. Sangid, H. Sehitoglu, Energy barriers associated with slip—twin interactions, Philosoph. Mag. 91 (2011) 1464–1488, doi: 10.1080/14786435.2010.541166.
- [3] Y.T. Zhu, X.L. Wu, X.Z. Liao, J. Narayan, L.J. Kecskés, S.N. Mathaudhu, Dislocation—twin interactions in nanocrystalline fcc metals, Acta Mater. 59 (2011) 812–821, doi: 10.1016/j.actamat.2010.10.028.
- [4] D. Wei, M. Zaiser, Z. Feng, G. Kang, H. Fan, X. Zhang, Effects of twin boundary orientation on plasticity of bicrystalline copper micropillars: A discrete dislocation dynamics simulation study, Acta Mater. 176 (2019) 289–296, doi: 10.1016/j.acta-mat.2019.07.007.
- [5] K. Lu, L. Lu, S. Suresh, Strengthening Materials by Engineering coherent internal boundaries at the nanoscale, Science 324 (2009) 349–352, doi: 10.1126/science.1159610.
- [6] M.W. Grabski, R. Korski, Grain boundaries as sinks for dislocations, Philosoph. Mag. J. Theor. Exper. Appl. Phys. 22 (1970) 707–715, doi: 10.1080/14786437008220941.
- [7] J. Kacher, B.P. Eftink, B. Cui, I.M. Robertson, Dislocation interactions with grain boundaries, Current Opin. Solid State Mater. Sci. 18 (2014) 227–243, doi: 10.1016/j.cossms.2014.05.004.
- [8] Z. You, X. Li, L. Gui, Q. Lu, T. Zhu, H. Gao, et al., Plastic anisotropy and associated deformation mechanisms in nanotwinned metals, Acta Mater. 61 (2013) 217– 227, doi: 10.1016/j.actamat.2012.09.052.
- [9] D. Jang, X. Li, H. Gao, J.R. Greer, Deformation mechanisms in nanotwinned metal nanopillars, Nature Nanotechnol. 7 (2012) 594–601, doi: 10.1038/nnano.2012.116.
- [10] M.D. Sangid, T. Ezaz, H. Sehitoglu, Energetics of residual dislocations associated with slip—twin and slip—GBs interactions, Mater. Sci. Eng. A 542 (2012) 21–30, doi: 10.1016/j.msea.2012.02.023.

- [11] D. Culbertson, Q. Yu, J. Wang, Y. Jiang, Pre-compression effect on microstructure evolution of extruded pure polycrystalline magnesium during reversed tension load, Mater. Character. 134 (2017) 41–48, doi: 10.1016/j.matchar.2017.10.003.
- [12] J. Wang, S.K. Yadav, J.P. Hirth, C.N. Tomé, I.J. Beyerlein, Pure-shuffle nucleation of deformation twins in hexagonal-close-packed metals, Mater. Res. Lett. 1 (2013) 126–132, doi: 10.1080/21663831.2013.792019.
- [13] P. Chen, F. Wang, J. Ombogo, B. Li, Formation of 60° (01-10) boundaries between {10-12} twin variants in deformation of a magnesium alloy, Mater. Sci. Eng. A 739 (2019) 173–185, doi: 10.1016/j.msea.2018.10.029.
- [14] P. Chen, B. Li, D. Culbertson, Y. Jiang, Contribution of extension twinning to plastic strain at low stress stage deformation of a Mg-3Al-1Zn alloy, Mater. Sci. Eng. A 709 (2018) 40–45, doi: 10.1016/j.msea.2017.10.038.
- [15] H. El Kadiri, A.L. Oppedal, A crystal plasticity theory for latent hardening by glide twinning through dislocation transmutation and twin accommodation effects, J. Mech. Phys. Solids 58 (2010) 613–624, doi: 10.1016/j.jmps.2009.12.004.
- [16] L. Capolungo, I.J. Beyerlein, G.C. Kaschner, C.N. Tomé, On the interaction between slip dislocations and twins in HCP Zr, Mater. Sci. Eng. A 513 (2009) 42–51, doi: 10.1016/j.msea.2009.01.035.
- [17] P. Chen, B. Li, D. Culbertson, Y. Jiang, Negligible effect of twin-slip interaction on hardening in deformation of a Mg-3Al-1Zn alloy, Mater. Sci. Eng. A 729 (2018) 285–293, doi: 10.1016/j.msea.2018.05.067.
- [18] P. Chen, F. Wang, B. Li, Dislocation absorption and transmutation at {10-12} twin boundaries in deformation of magnesium, Acta Mater. 164 (2019) 440–453, doi: 10.1016/j.actamat.2018.10.064.
- [19] A. Serra, D.J. Bacon, R.C. Pond, Twins as barriers to basal slip in hexagonal-close-packed metals, Metall Mat. Trans. A 33 (2002) 809–812, doi: 10.1007/s11661-002-0149-7
- [20] F. Wang, S.R. Agnew, Dislocation transmutation by tension twinning in magnesium alloy AZ31, Int. J. Plast. 81 (2016) 63–86, doi: 10.1016/j.ijplas.2016.01.012.
- [21] A. Serra, D.J. Bacon, Computer simulation of screw dislocation interactions with twin boundaries in H.C.P. metals, Acta Metallurg. et Mater. 43 (1995) 4465–4481, doi: 10.1016/0956-7151(95)00128-I.
- [22] F. Hiura, R.K. Mishra, M. Lukitsch, M. Niewczas, Nano-Indentation Studies of Twinned Magnesium Single Crystals, Magnesium Technology, 2012, Springer, Cham, 2012, pp. 117–119, doi: 10.1007/978-3-319-48203-3_22.
- [23] B. Li, X.Y. Zhang, Twinning with zero twinning shear, Scripta Mater. 125 (2016) 73–79, doi: 10.1016/j.scriptamat.2016.07.004.
- [24] X.Y. Zhang, B. Li, X.L. Wu, Y.T. Zhu, Q. Ma, Q. Liu, et al., Twin boundaries showing very large deviations from the twinning plane, Scripta Mater. 67 (2012) 862–865, doi: 10.1016/j.scriptamat.2012.08.012.
- [25] C. Cayron, R. Logé, Evidence of new twinning modes in magnesium questioning the shear paradigm, J. Appl. Crystallogr. 51 (2018) 809–817, doi: 10.1107/ \$1600576718005678.
- [26] S.G. Song, G.T. Gray, Structural interpretation of the nucleation and growth of deformation twins in Zr and Ti–II. Tem study of twin morphology and defect reactions during twinning, Acta Metallurg. et Mater. 43 (1995) 2339–2350, doi: 10.1016/0956-7151(94)00434-X.
- [27] S.G. Song, G.T. Gray, Structural interpretation of the nucleation and growth of deformation twins in Zr and Ti—I. Application of the coincidence site lattice (CSL) theory to twinning problems in H.C.P. structures, Acta Metallurg. et Mater. 43 (1995) 2325–2337, doi: 10.1016/0956-7151(94)00433-1.
- [28] B. Li, E. Ma, Zonal dislocations mediating {101-1}(10-1-2) twinning in magnesium, Acta Mater. 57 (2009) 1734–1743, doi: 10.1016/j.actamat.2008.12.016.
- [29] Y.M. Zhu, S.W. Xu, J.F. Nie, {10-11} Twin boundary structures in a Mg-Gd alloy, Acta Materialia 143 (2018) 1-12, doi: 10.1016/j.actamat.2017.09.067.
- [30] A. Chakkedath, T. Maiti, J. Bohlen, S. Yi, D. Letzig, P. Eisenlohr, et al., Contraction twinning dominated tensile deformation and subsequent fracture in extruded Mg-1Mn (Wt Pct) at ambient temperature, Metall. Mat. Trans. A 49 (2018) 2441– 2454. doi: 10.1007/s11661-018-4557-8.
- [31] M. Knezevic, A. Levinson, R. Harris, R.K. Mishra, R.D. Doherty, S.R. Kalidindi, Deformation twinning in AZ31: Influence on strain hardening and texture evolution, Acta Mater. 58 (2010) 6230–6242, doi: 10.1016/j.actamat.2010.07.041.
- [32] Q. Peng, Y. Sun, B. Ge, H. Fu, Q. Zu, X. Tang, et al., Interactive contraction nanotwins-stacking faults strengthening mechanism of Mg alloys, Acta Mater. 169 (2019) 36–44, doi: 10.1016/j.actamat.2019.02.040.
- [33] H. Fu, B. Ge, Y. Xin, R. Wu, C. Fernandez, J. Huang, et al., Achieving High Strength and Ductility in Magnesium Alloys via Densely Hierarchical Double Contraction Nanotwins, Nano Lett. 17 (2017) 6117–6124, doi: 10.1021/acs.nanolett.7b02641.
- [34] M. Yuasa, K. Masunaga, M. Mabuchi, Y. Chino, Interaction mechanisms of screw dislocations with and twin boundaries in Mg, Philosoph. Mag. 94 (2014) 285– 305, doi: 10.1080/14786435.2013.853136.
- [35] Z. Li, J. Wang, W. Liu, Basal (a) dislocation-{1011} contraction twin interactions in magnesium, Comput. Mater. Sci. 155 (2018) 11–16, doi: 10.1016/j.commatsci.2018.08.034.
- [36] M.S. Daw, M.I. Baskes, Semiempirical, Quantum Mechanical Calculation of Hydrogen Embrittlement in Metals, Phys. Rev. Lett. 50 (1983) 1285–1288, doi: 10.1103/ PhysRevLett.50.1285.
- [37] M.S. Daw, M.I. Baskes, Embedded-atom method: Derivation and application to impurities, surfaces, and other defects in metals, Phys. Rev. B. 29 (1984) 6443– 6453, doi: 10.1103/PhysRevB.29.6443.
- [38] X.-Y. Liu, J.B. Adams, F. Ercolessi, J.A. Moriarty, EAM potential for magnesium from quantum mechanical forces, Modell. Simul. Mater. Sci. Eng. 4 (1996) 293, doi: 10.1088/0965-0393/4/3/004.
- [39] B.-Y. Liu, J. Wang, B. Li, L. Lu, X.-Y. Zhang, Z.-W. Shan, et al., Twinning-like lattice reorientation without a crystallographic twinning plane, Nat Commun. (2014) 5, doi: 10.1038/ncomms4297.

- [40] B. Li, E. Ma, Pyramidal slip in magnesium: Dislocations and stacking fault on the {1011} plane, Philosoph. Mag. 89 (2009) 1223–1235, doi: 10.1080/14786430902936707.
- [41] P. Chen, F. Wang, B. Li, Misfit strain induced phase transformation at a basal/prismatic twin boundary in deformation of magnesium, Comput. Mater. Sci. 164 (2019) 186–194, doi: 10.1016/j.commatsci.2019.04.020.
- [42] A. Stukowski, Visualization and analysis of atomistic simulation data with OVI-TO-the Open Visualization Tool, Modell. Simulat. Mater. Sci. Eng. 18 (2010) 015012, doi: 10.1088/0965-0393/18/1/015012.
- [43] J.Dana. Honeycutt, H.C. Andersen, Molecular dynamics study of melting and freezing of small Lennard-Jones clusters, J. Phys. Chem. 91 (1987) 4950–4963, doi: 10.1021/j100303a014.
- [44] E. Kelley, W. Hosford, Plane-strain compression of magnesium and magnesium alloy crystals, Trans. Met. Soc. AIME 242 (1968) 5–13.
- [45] Q. Sun, Q. Zhang, B. Li, X. Zhang, L. Tan, Q. Liu, Non-dislocation-mediated basal stacking faults inside 101–1 twins, Scripta Mater. 141 (2017) 85–88, doi: 10.1016/j.scriptamat.2017.07.036.
- [46] J.W. Christian, S. Mahajan, Deformation twinning, Progress Mater. Sci. 39 (1995) 1–157.
- [47] J.W. Christian, The theory of transformations in metals and alloys, Newnes (2002).
- [48] Z.S. Basinski, M.S. Szczerba, M. Niewczas, J.D. Embury, S.J. Basinski, The transformation of slip dislocations during twinning of copper-aluminum alloy crystals, Rev. Met. Paris 94 (1997) 1037–1044, doi: 10.1051/metal/199794091037.
- [49] M. Niewczas, Lattice correspondence during twinning in hexagonal close-packed crystals, Acta Mater. 58 (2010) 5848–5857, doi: 10.1016/j.actamat.2010.06.059.
- [50] S. Vaidya, S. Mahajan, Accommodation and formation of {11-21} twins in Co single crystals, Acta Metallurg. 28 (1980) 1123–1131.

- [51] H. Fan, S. Aubry, A. Arsenlis, J.A. El-Awady, The role of twinning deformation on the hardening response of polycrystalline magnesium from discrete dislocation dynamics simulations, Acta Mater. 92 (2015) 126–139, doi: 10.1016/j.actamat.2015.03.039.
- [52] X.Y. Zhang, B. Li, J. Tu, Q. Sun, Q. Liu, Non-classical twinning behavior in dynamically deformed cobalt, Mater. Res. Lett. 3 (2015) 142–148, doi: 10.1080/21663831.2015.1034297.
- [53] X.Y. Zhang, B. Li, Q. Sun, On the {10-12} "twinning shear" measured from line deflection, Scripta Mater. 159 (2019) 133–136, doi: 10.1016/j.scriptamat.2018.09.027.
- [54] B. Li, E. Ma, Atomic Shuffling Dominated Mechanism for Deformation Twinning in Magnesium, Phys. Rev. Lett. 103 (2009) 035503, doi: 10.1103/PhysRev-Lett.103.035503.
- [55] P. Chen, F. Wang, B. Li, Transitory phase transformations during {10-12} twinning in titanium, Acta Mater. 171 (2019) 65–78, doi: 10.1016/j.actamat.2019.04.002.
- [56] J.P. Hirth, J. Wang, C.N. Tomé, Disconnections and other defects associated with twin interfaces, Progress Mater. Sci. 83 (2016) 417–471, doi: 10.1016/j. pmatsci.2016.07.003.
- [57] H.A. Khater, A. Serra, R.C. Pond, Atomic shearing and shuffling accompanying the motion of twinning disconnections in Zirconium, Philosoph. Mag. 93 (2013) 1279–1298, doi: 10.1080/14786435.2013.769071.
- [58] C.D. Barrett, H. El Kadiri, The roles of grain boundary dislocations and disclinations in the nucleation of {10-12} twinning, Acta Mater. 63 (2014) 1-15, doi: 10.1016/j.actamat.2013.09.012.
- [59] Q. Zu, X.-Z. Tang, H. Fu, Q.-M. Peng, Y.-F. Guo, The irrational shear of {1011} twinning in Mg, Materialia 5 (2019) 100239, doi: 10.1016/j.mtla.2019.100239.